AD-A062 759 UNIVERSITY COLL OF NORTH WALES BANGOR SCHOOL OF ELEC--ETC F/G 7/4
A STUDY OF THE NATURE AND ORIGIN OF PYROELECTRICITY AND PIEZOEL--ETC(U)
AUG 78 D K DAS-GUPTA DA-ERO-78-G-004

UNCLASSIFIED NL

| OF |
AD
A062759

END
DATE
FILMED
3-79
DDC

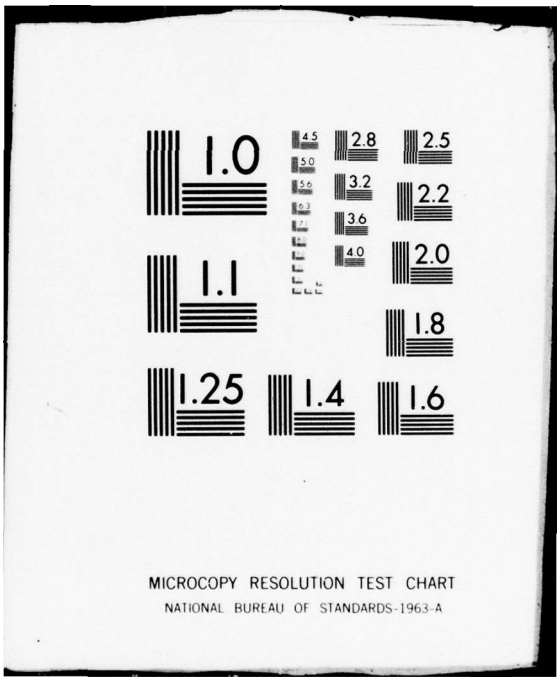
1.0
1.1
1.25
4.5
5.0
5.6
6.3
2.8
3.2
3.6
4.0
2.5
2.2
2.0
1.8
1.4
1.6
MICROCOPY RESOLUTION TEST CHART
NATIONAL BUREAU OF STANDARDS-1963-A

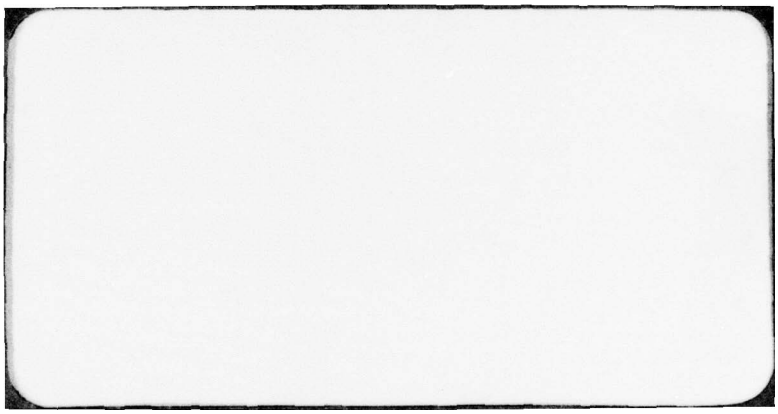

(16) 1T161102BH57

(17) 03.00

(6) A STUDY OF THE NATURE AND ORIGIN OF PYROELECTRICITY AND PIEZOELECTRICITY IN POLYVINYLIDENEFLUORIDE AND ITS COPOLYMER WITH TETRAFLUOROETHYLENE

First Annual Technical Report

by

(10) Dr. D. K. Das-Gupta

(11) August 1978

(12) 67 p.

(9) Annual Technical rept. no. 1, Sep 77 - Aug 78,

EUROPEAN RESEARCH OFFICE

United States Army

London NW1 England

(15) DA-ERO-78-G-004

GRANT NUMBER DA-ERO-~~78-G-008~~ 78-G-004

School of Electronic Engineering Science,
University College of North Wales,
Dean Street, Bangor, Gwynedd, LL57 1UT, U.K.

New

Approved for Public Release; distribution unlimited

410993

UNCLASSIFIED

SECURITY CLASSIFICATION OF THIS PAGE (When Data Entered)

R&D 2437

REPORT DOCUMENTATION PAGE

READ INSTRUCTIONS BEFORE COMPLETING FORM

1. REPORT NUMBER	2. GOVT ACCESSION NO. / 3. RECIPIENT'S CATALOG NUMBER
4. TITLE (and Subtitle): A Study of the Nature and Origin of Pyroelectricity and Piezoelectricity in Polyvinylidenefluoride and its Copolymer with Tetrafluoroethylene.	5. TYPE OF REPORT & PERIOD COVERED: Annual Tech. Report Sep 77 - Aug 78
	6. PERFORMING ORG. REPORT NUMBER
7. AUTHOR(s): Dr. D.K. Das-Gupta	8. CONTRACT OR GRANT NUMBER(s): DAERO-~~77-G-008~~ 78-G-004
9. PERFORMING ORGANIZATION NAME AND ADDRESS: School of Electronic Engineering Sciences, University College of North Wales, Bangor, U.K.	10. PROGRAM ELEMENT, PROJECT, TASK AREA & WORK UNIT NUMBERS: 6.11.02A-1T161102BH57-03-00-689
11. CONTROLLING OFFICE NAME AND ADDRESS: U.S. Army R&S Gp (Eur), Box 65, FPO NY 09510	12. REPORT DATE: Sep 78
	13. NUMBER OF PAGES: 64
14. MONITORING AGENCY NAME & ADDRESS (if different from Controlling Office)	15. SECURITY CLASS. (of this report): UNCLASSIFIED
	15a. DECLASSIFICATION/DOWNGRADING SCHEDULE

16. DISTRIBUTION STATEMENT (of this Report)

Approved for Public Release; Distribution Unlimited.

17. DISTRIBUTION STATEMENT (of the abstract entered in Block 20, if different from Report)

18. SUPPLEMENTARY NOTES

19. KEY WORDS (Continue on reverse side if necessary and identify by block number)

Polymers, Polyvinylidenefluoride, Tetrafluoroethylene, Pyroelectricity, Piezoelectricity, Charge Storage.

microns

20. ABSTRACT (Continue on reverse side if necessary and identify by block number)

X-ray diffraction profiles, piezoelectric strain coefficient d_{31} and the pyroelectric coefficient P_3 of 50um (Form 2 crystallites only) and 25um (both Form 1 and Form 2 crystallites) thick PVF_2 films have been studied after (i) corona poling (ii) uniaxial stretching and (iii) uniaxial stretching and corona poling. The results suggest that the induced piezo- and pyroelectricity in PVF_2 is of dipolar origin. However, there is a difference in a sense that corona poling alone at fields →

DD FORM 1 JAN 73 1473 EDITION OF 1 NOV 65 IS OBSOLETE

UNCLASSIFIED

SECURITY CLASSIFICATION OF THIS PAGE (When Data Entered)

20.

$3 \times 10^{8} Vm^{-1}$ produces mainly an intermediate polar form of Form 2 crystallites by a co-operative rotation of the alternate polymer chains through 180° about the chain axis (i.e. c-axis) without losing its T-G-T-G' molecular conformation and the unit cell dimensions remaining unaltered. Uniaxial stretching, however, produces a direct conversion to the polar Form 1 type of structure from the non-polar Form 2 crystallites. A study of birefringence and small angle light scattering (SALS) patterns has also been made with uniaxially stretched PVF_2 films, originally containing only Form 2 (non-polar) crystallites. The results indicate that the major contribution to the observed orientation, producing Form 1 type polar crystallites, originates from the crystallite regions of the polymer.

degrees

1/3 x 10 to the 8th power Vm

Summary

X-ray diffraction profiles, piezoelectric strain coefficient d_{31} and the pyroelectric coefficient p_3 of 50μm (Form 2 crystallites only) and 25μm (both Form 1 and Form 2 crystallites) thick PVF_2 films have been studied after (i) corona poling (ii) uniaxial stretching and (iii) uniaxial stretching and corona poling. The results suggest that the induced piezo- and pyroelectricity in PVF_2 is of dipolar origin. However, there is a difference in a sense that corona poling alone at fields $\gtrless 3\times10^{8} Vm^{-1}$ produces mainly an intermediate polar form of Form 2 crystallites by a co-operative rotation of the alternate polymer chains through 180^{o} about the chain axis (i.e. c-axis) without losing its T-G-T-G' molecular conformation and the unit cell dimensions remaining unaltered. Uniaxial stretching, however, produces a direct conversion to the polar Form 1 type of structure from the non-polar Form 2 crystallites. A study of birefringence and small angle light scattering (SALS) patterns has also been made with uniaxially stretched PVF_2 films, originally containing only Form 2 (non-polar) crystallites. The results indicate that the major contribution to the observed orientation, producing Form 1 type polar crystallites, originates from the crystallite regions of the polymer.

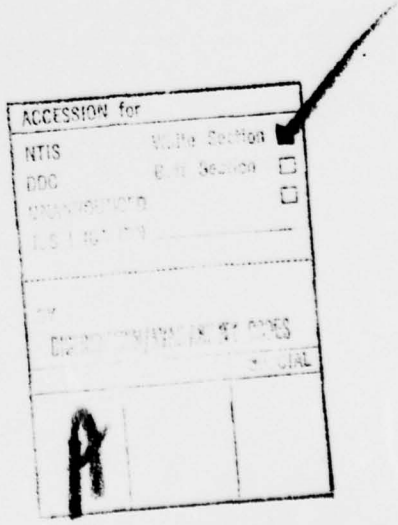

TABLE OF CONTENTS

1. Introduction

Polyvinylidenefluoride (PVF_2) may be made to exhibit piezo- and pyroelectric responses significantly greater than those of other commercially available films of polymers after suitable poling. The established poling procedure (i.e. conventional poling) is to subject a metal-polymer-metal system to a very high electrical stress at an elevated temperature for an extended period of time and then to reduce the temperature of the specimen to $\sim 20^{\circ}C$ (i.e. ambient temperature) before removing the external field. The exact nature of the poling and the origin of the piezo- and pyroelectricity in PVF_2 are, however, not yet understood. Wada and Hayakawa[1] suggest that the piezo- and pyroelectricity in the material may be due to one of the following mechanisms, (i) strain and temperature dependence of spontaneous polarization (i.e. a dipolar model) and (ii) heterogeneity and embedded charges in the bulk of the polymer.

PVF_2 may exist at lease in two stable polymorphs. In Form 1 (β-form) polar structure, the molecules have a planar zig-zag conformation and the orthorhombic base-centred unit cell with two polymer chains has the space group $Cm2m(C_{2v}^{14})$, the lattice constants being a = 8.58Å, b = 4.91Å and c = 2.56Å (figure 1).[2,3] In the Form 1 structure the dipole moments of the monomer units ($-CH_2-CF_2-$) in a poled film are aligned parallel to each other along the b-axis, the magnitude of the dipole moment[4] for each monomer unit being 7.0×10^{-30} C-m. Assuming a rigid dipolar model the spontaneous polarization of a single crystal[1] of the Form 1 type PVF_2 will be 0.13 $C\text{-}m^{-3}$ and it will exhibit piezoelectricity without any external poling. Form 2 crystallites (α-form) have a space group of $P_{21}/C(C_{2h}^{5})$ with a primitive monoclinic unit cell structure, the lattice parameters being[3] a = 4.96Å, b = 9.64Å, c = 4.62Å and $\beta = 90^{\circ}$ (figure 2). Although each molecular chain with T-G-T-G' conformation of the Form 2 structure has a dipole moment

normal to the chain-axis, however, the adjacent chains pack with their dipoles in an antipolar array (see figure 2). As a result, the unit cell of Form 2 structure has no net dipole moment along the b-axis. Thus PVF_2 films of Form 2 structure may not be expected to be piezoelectric. The Form 2 structure may be transformed into Form 1 type crystallites on uniaxial stretching of PVF_2 films at a temperature $\sim 60^{\circ}C$. However, the piezoelectric response of such stretched films will be negligible without subsequent poling. This may be attributed to the fact that although the process of uniaxial stretching results in an orientation of the c-axis of the crystalline region parallel to the stretch direction, however, due to orthorhombic symmetry of the unit cell, the rotation of the unit cell axes can be accomplished in six possible variations (i.e. 60° increments) without disruption of the polymer morphology. Murayama et al[6] show that in PVF_2 films containing both forms of crystallites, the piezoelectric response increases with increasing Form 1 content. Due to the symmetry properties of the point group mm2 for the uniaxially stretched and poled PVF_2 films the non-zero matrix elements of the piezoelectric strain coefficients are $+d_{15}$, $+d_{24}$, $+d_{31}$, $+d_{32}$ and $-d_{33}$, where the first and the second subscripts refer to the direction coordinates of polarization and stress respectively. The corresponding pyroelectric coefficient is $-p_3$. It may be noted that Ohigashi[8] has shown that a large piezoelectric strain coefficient d_{33} may be obtained by poling PVF_2 films containing mostly the nonpolar Form 2 crystallites. This observation apparently suggests that the dipolar orientation may not be the origin of piezoelectricity in PVF_2. On the other hand, the observations of the hysteresis loop with the piezo- and pyroelectric coefficients in PVF_2 under the dc bias fields[9-12] with reproducible residual polarization[1,13] would tend to favour the dipolar model. There is thus, as yet, no definitive knowledge of the nature and origin of pyroelectricity in PVF_2.

From the results shown in the First Periodic Status Report (September

1977 - February 1978) it may be observed that the corona charging is an effective method of poling of PVF_2 films. The present report shows the results of a study of structural changes and the behaviour of d_{31} on (i) drawing, (ii) poling (conventional and corona charging) and corona charging PVF_2 films, originally containing mostly Form 2 crystallites. The experimental details of the corona charging, X-ray diffraction analysis and the measurement of d_{31} have already been described in the 'First Terminal Report'.

2. Results

2.1 X-ray Diffraction Profile with 50μm thick Kureha PVF_2 films of Form 2 structure

Figure 3 shows a typical X-ray diffraction profile of Form 2 PVF_2 films in the range of (Bragg angle) 10-30°. The crystallinity of the film was determined from such a diffraction profile using a method due to Gal'perin[14] and it was observed to be ∿52% at room temperature. Figure 4 shows the behaviour of the crystallinity of the Form 2 samples with temperature. The crystallinity was observed to return to the value of 52% on cooling of the sample from 100°C to room temperature. Typical diffraction profiles of Form 2 peaks at different temperatures are shown in figure 5. Figure 6 shows the changes in the interplanar spacings, i.e. a- and b- lattice spacings which were calculated from such diffraction profiles as shown in figure 5 and the observed pattern of thermal expansion is in agreement with the results of Nakagawa and Ishida.[15]

The changes in the diffraction profiles of PVF_2 films of Form 2 structure due to corona charging (positive corona) at surface potentials of 10 and 15KV are shown in figure 7. A diffraction profile of the unpoled polymer is also superimposed in figure 7 for the sake of comparison. Figure 8 shows a typical behaviour of the observed peak heights of the structural planes (100), (020) and (110) with corona poling potentials. Figures 9 and 10 show the behaviour of the higher order diffraction profiles

of Form 2 structure with corona poling in the 2θ range (Bragg angle) of 25.5 - 34° and 35 - 40° respectively. Figure 11 gives the diffraction profile after corona poling at a near breakdown surface potential of 18KV at 20°C which offers the evidence of the occurrence of a conversion from Form 2 to Form 1 type of structure. At higher temperatures such a conversion may occur at lower corona fields which may be evidenced from figure 12. It should also be noted that a corona poling of Form 2 structure may occur even at a temperature of -80°C (figure 13) which is below its glass transition temperature (Tg).

2.2 Piezoelectric Coefficient d_{31}, of Corona Charged films of Form 2 structure

Figure 14 shows the behaviour of d_{31} after corona charging at different poling surface potentials and at different temperatures. The effect of poling time (corona charging) at different temperatures on the magnitude of d_{31} is illustrated in figure 15 from which it may be observed that the increase in magnitude of d_{31} at temperatures <100°C with increasing poling time is not very significant.

2.3 Structural Changes with corona poling in 25μm thick Kureha films containing both the Form 1 and Form 2 types of crystallites

Figure 16 shows the structural changes induced by corona poling of PVF_2 films originally containing both Form 1 and Form 2 types of crystallites. Figures 17 and 18 show the effects of increasing the poling fields on higher order peaks in the range of Bragg angles 25 - 34° and 35 - 37.5° respectively. Figures 19 and 20 show the behaviour of peak intensities of the major peaks after corona poling as functions of poling fields at 20° and 100°C respectively. It may be mentioned that the thermal expansion behaviour of both the 50μm (Form 2 type) and 25μm (Form 1 and Form 2 types) thick Kureha films are similar, which may be evidenced from figure 21 which shows a comparison of the variations of peak heights

of (110) Form 2 and |(110)+(200)| of Form 1 types of crystallites at different temperatures.

2.4 Piezoelectric coefficient d_{31}, of corona poled PVF_2 films of 25μm thickness containing both the Form 1 and Form 2 types of crystallites

The behaviour of d_{31} after poling with different surface potentials (corona charging) as a function of poling time is shown in figure 22, from which it may be observed that the magnitude of d_{31} does not increase significantly for poling for a period in excess of 200s at room temperature. Figure 23 shows the effect of poling temperature on the magnitude of d_{31} for different poling fields (corona charging). No significant improvement in d_{31} was observed for a poling potential of 7.5KV at temperatures in excess of 60°C.

In the experiments described above, poling was achieved using positive corona charges. However, the magnitude of d_{31} was observed to be independent of the polarity of the corona charges which may be observed from figure 24.

Most of the corona poling was achieved using aluminium electrodes. However, limited work was carried out with gold and silver dag electrodes. Figure 25 shows that the magnitude of d_{31} is independent of electrode materials used in the present work.

Figure 25 shows the effect of cooling the specimen in the presence of the corona poling field on d_{31} at different temperatures for two different poling potentials (i.e. 2.5 and 7.5KV). It may be noticed (figure 26) that d_{31} is enhanced if the sample is cooled in the presence of the corona charging for the case of low poling potential only.

Perhaps it should be mentioned that the magnitudes of d_{31} for 50μm (Form 2 type) and 25μm (Form 1 + Form 2) are comparable at high poling fields.

2.5 X-ray diffraction profile of stretched and corona charged PVF_2 films

On uniaxial stretching of 50μm thick (originally Form 2 type of crystallites), as expected, a molecular conformational change occurs in the polymer, giving rise to a Form 1 type of structure which may be evidenced in figure 27 by the (i) presence of dominant (110)/(200) composite peak and (ii) the absence of the former Form 2 (110) peak. On corona charging of the stretched film the composite (110)/(200) of the Form 1 type structure was observed to be further enhanced (figure 27). Similar behaviour was also observed with 22.5μm thick PVF_2 films, originally containing both Form 1 and Form 2 type crystallites (see figures 28 and 29). Figures 30 and 31 show the behaviour of d_{31} after stretching and corona poling of 50μm (Form 2) and 22.5μm (Form 1 + Form 2) thick PVF_2 films. It may be noticed from these results that the magnitude of d_{31} may be significantly improved by stretching the films before corona charging. Figures 32 and 33 show the behaviour of d_{31} with stretched 22.5μm (Form 1 + Form 2) after (i) conventional poling and (ii) corona charging respectively.

The piezoelectric strain coefficient d_{31} was measured by the conventional technique of the release of a standard weight by an electro-pneumatic relay in a temperature controlled oven and recording the voltage developed (due to charge release) across a standard mica capacitor with a storage oscilloscope.

2.6 Pyroelectric coefficient of corona poled 25μm (originally of Form 1 + Form 2 structure) thick PVF_2 films

A typical behaviour of thermally stimulated (short circuited) currents (TSC) for the first heating cycle with PVF_2 films, poled at two different surface potentials of 5 and 10KV (positive corona) are shown in figure 34. Both curves display a broad peak at $\sim 49^{\circ}C$ and have similar

profiles to those reported by other workers[16,17,18]. In figure 35 are presented the typical behaviour of the true (i.e. reversible) pyroelectric currents for the second and successive cycles with temperature, which are about an order magnitude lower than those for the TSC currents (irreversible), observed during the first cycle (figure 34). The pyroelectric coefficient p in curve A (figure 35, 10KV case) appears to be $\sim 3\times10^{-5} C/m^2K$ at 20°C, rising to a value of $8\times10^{-5} C/m^2K$ at 90°C. The corresponding values of p for curve B (figure 35, 5KV case) are $\sim 2\times10^{-5} C/m^2K$ and $6\times10^{-5} C/m^2K$ respectively. One largest yet reported magnitude of p at room temperature for conventionally poled PVF_2[9] is $4.1\times10^{-5} C/m^2K$ which is in good agreement with the present work in which corona poling has been employed. The magnitude of p seems to increase linearly (figure 35) with temperature up to ~60°C beyond which there is evidence of super-linear rate of increase which is also in agreement with other workers.[18,20]

2.7 Measurement of Birefringence and the Small Angle Light Scattering of 50μm (Form 2) patterns as a function of stretch ratio

50μm thick films (mostly of Form 2 crystal structure) of PVF_2 were uniaxially stretched at 60°C and then annealed at 120°C. A He-Ne laser beam was employed for studying changes in birefringence and SALS (small angle light scattering) patterns in the H_v scattering mode (i.e. crossed polarizers). The optical system employed in the present work is shown in figure 36 which is similar to that of Stein and Rhodes.[21] The total birefringence was determined by the Senarmont Method[22] which utilises an analyser quarter wave plate between the crossed polarizers in the H_v mode. Figures 37 and 38 show the changes in the birefringence and the SALS patterns respectively with different stretch ratios.

3. Discussion

The diffraction profile of unstretched and unpoled PVF_2 films of both 50μm (mostly containing Form 2 crystallites) and 25μm (Form 1 + Form 2

crystallites) which are shown in figures 3, 16, are in good agreement with Hasegawa et al.[3] For the 50μm (Form 2) thick sample, it may be observed from figures 6-9 that the diffracted intensities of the Form 2 structural planes (100), (020), (021) and (130) become vanishingly small with corona charging. Furthermore, the peak intensities of the Form 2 (110) and (200) planes increase with increasing poling fields (figures 7, 8, 10 and 11). Similar changes also occur[23] on corona poling of PVF_2 films 25μm thick containing both Form 1 and Form 2 crystallites (figures 16 - 20). However, it may be observed from figure 7 that even with the very high poling field of $3\times10^{8}Vm^{-1}$ (i.e. 15KV case) there is no apparent evidence of a transformation from Form 2 (non-polar) crystallite to a polar Form 1 structure. At the same time, it may be observed from figure 14 that a very significant enhancement in the magnitude of d_{31} occurs on corona poling of PVF_2 films of Form 2 structure, reaching a value of $7\times10^{-12}CN^{-1}$ at a poling field of $3\times10^{8}Vm^{-1}$ (i.e. surface potential of 15KV). It has been stated that using a dipolar model an antipolar unit cell of Form 2 structure may not give rise to piezoelectricity. Furthermore, the depolarisation current studies in PVF_2 films[25] with respect to the variable parameters, viz., poling fields, time, temperature, electrode thickness and electrode materials, indicate no significant evidence of charge injection from the electrodes leading to space charge formation in the bulk of the polymer at such high fields. Therefore, in view of the observed results in figures 7-10 and 14, it is suggested that a structural transformation of the non-polar form to an intermediate polar form without any alteration of the lattice dimensions of the Form 2 structure (see figure 39) must occur on corona poling in PVF_2 films, originally containing mostly Form 2 crystallites. Such a conversion to an intermediate polar form but still maintaining the T-G-T-G' conformation of the molecular chain may occur on poling by only a rotation of the alternate molecular chain about the c-axis (i.e. the chain axis) through 180^{o}, which is illuatrated in figure 39. The stability of this intermediate polar form with the lattice dimensions of the Form 2 unit

cell structure, would not violate the conditions required for the minimum potential energy.[26,27] Such a model will also explain the observed reduction of the reflection-diffraction patterns of the Form 2 (100), (020), (021) and (130) planes (figures 7, 8 and 9). The model will also be in agreement with the results[24] obtained with corona poling of 25μm thick PVF_2 films containing both Form 1 and Form 2 crystallites (figures 16-20). Figure 11 shows that at still higher fields of $3.6\times10^{8}Vm^{-1}$ (surface potential of 18KV) a conformational change may occur in which the intermediate polar Form 2 crystallites finally proceed to be converted to the polar zig-zag type Form 1 crystallite. This is evidenced by the presence of a broad diffraction profile of the composite Form 1 (110)+(200) planes (figure 11) which is also in agreement with Davis et al[27] and Das-Gupta and Doughty.[24]

On uniaxial stretching of PVF_2 films only a conformational change occurs from Form 2 type of crystallites to Form 1 type (figure 27) in which the crystallites are oriented at random i.e., fix possible variations with 60^{o} increments) rotational angles about the c-axis, giving no net dipole moments. The dipole moments can, however, be oriented at an angle with respect to the electric field during the poling process in which the peak height of the diffraction profile of the Form 1 composite peak (100)+(200) planes is further enhanced (figures 28 and 29).

Thus it may be suggested that the induced piezoelectricity due to corona poling alone at fields up to $\sim3\times10^{8}Vm^{-1}$ of PVF_2 films, originally containing mostly Form 2 type of crystallites, is due to a cooperative rotation of the alternate polymer chains about the c-axis which produces a stable polar form still maintaining the T-G-T-G' molecular conformation and the lattice parameters of the Form 2 crystallites. At fields higher than $3\times10^{8}Vm^{-1}$ there is a progressive conversion of the Form 2 crystallites into the Form 1 type of structure with the zig-zag molecular conformation. On

the other hand, on uniaxial stretching of the polymer there is a direct conversion of the crystallites from the Form 2 structure to that of Form 1 with randomly oriented dipoles. On subsequent poling the dipoles align, of course, at a particular angle with the direction of the poling field. The dominant mechanism of piezoelectricity in this polymer remains, however, of dipolar origin.

The magnitude of d_{31}, observed in the present work, with the corona poled samples, is in agreement with that observed by other workers who[56] used conventional poling technique at comparable electrical stresses.

Wada and Hayakawa[1] observe that the unit cell structure of Form 1 crystal has a large spontaneous polarization P_s, of $0.13C/m^2$ which increases with increasing poling field. An integration of the liberated (irreversible) charges for the first TSC runs for the curves A and B in figure 34 yields polarization values of ~ 0.02 and $0.01C/m^2$ respectively. Pfister et al[29] show that such irreversible polarization is approximately proportional to the (conventional) poling field which is in agreement with the present work where corona poling was employed. The activation energies, calculated from the initial slope to the peak positions[30] of the curves A and B in figure 34 were found to be 1.4 and 1.2eV. For these calculations (i.e. polarization and activation energies) the reversible pyroelectric currents (figure 35) were subtracted from the irreversible TSC curves (figure 34) of the first cycles. The values obtained for the activation energies in this work are lower than those due to Sharp and Garn[19] who, however, point out that the position and the magnitude of TSC peaks are dependent on the time interval between the poling and the measurement, i.e. 'rest-time'. The activation energy values would indicate the energy levels of the traps in the bulk of the polymer from which space charges are irreversibly liberated during the first cycle of the TSC run.

An integration of the pyroelectric currents in curves A and B

from 20 to 90°C (figure 35) produces values ∿0.004 and 0.002C/m^2 respectively for the residual polarization P_r, in the bulk of the polymer, which are about 20% of the magnitudes of the irreversible space charge polarization (curves A and B, figure 34). These values of P_r are similar to those obtained by Oshiki and Fukada.[13] Using a rigid dipole model Lines and Glass[31] estimate for the pyroelectric coefficient:

$$p = 0.07E \times 10^{-5} C/cm^2K \qquad \ldots\ldots \quad (1)$$

where E is in $10^8 Vm^{-1}$. The experimentally observed values of p in the present work (curves A and B, figure 35) are considerably higher than those predicted by equation (1). Thus the assumption of rigid dipoles may not be valid which is in agreement with Lines and Glass[30] who further add that a rotation of C-F and C-H bonds with temperature may be the dominant mechanism for pyroelectricity in PVF_2. In this respect a small change in the X-ray pole figure has indeed been noticed by Kepler et al[31] after poling Form 1 type PVF_2 films. It may also be noted that the crystallinity of polyethylene was observed to decrease from 67% to 57% on increasing the temperature from 25 to 110°C.[32] Following this argument Kepler and Anderson[5] that if similar changes in crystallinity were to occur in PVF_2, the magnitude of the pyroelectric coefficient would be $5.9 \times 10^{-5} C/m^2K$. In the present work, the crystallinity of Form 2 type PVF_2 (50μm thick) was estimated to change from ∿55% to 48% on heating the polymer film from 20 to 90°C (figure 4). These values are not significantly different from those for polyethylene and further investigations will be necessary in this respect. Tamura et al[33], on the other hand, suggest that the origin of piezo- and pyroelectricity in PVF_2 is dipolar orientation of the Form 1 types of crystals, embedded in the amorphous phase, along the direction of the poling field. They, however, add that the occurrence of such an orientation may be subject to the degree of crystallinity and the crystallite size. The polarity of p was observed to be opposite to that of d_{31} in the present work.

Following Nakamura and Wada[4] it may then be argued that the origin of the two phenomena in this polymer is dipolar orientation and not embedded true charges, distributed asymmetrically in the bulk. There is, however, a possibility that a part of the pyroelectricity observed in this polymer may, in fact, be of secondary nature, arising due to piezoelectricity when the specimen undergoes thermal expansion against its constraints. Such a possibility has been discussed by Kepler and Anderson.[5] The magnitudes of p and d_{31} were observed to be linearly related with each other in the present work for identical poling conditions. This is in agreement with other workers[12,34] who employed the conventional poling technique.

In the discussion so far it has been stressed that the dipolar orientations only in the crystalline region contribute to piezoelectricity in PVF_2. It has been suggested[33] that a dipolar alignment may be strongly influenced by the segmental motions in the amorphous regions in a semi-crystalline polymer such as PVF_2. Generally, crystalline polymers are volume filled with spherulites consisting of branched crystalline lamellae of folded chain crystals propagating from their centres.[35] The amorphous regions reside within these spherulites in the interlamellar areas. Such polymers deform on elongation when the spherulites change from the spherical into ellipsoidal shapes. This results in a change in the interlamellar spacing which leads to orientation of the amorphous materials between the lamellae. Now, the birefringence of a semicrystalline polymer provides useful information of the preferred overall orientation of the crystallites in both the crystalline and the amorphous regions. The results of the birefringence measurements on elongation up to a stretch ratio ~350%, shown in figure 37, are in good agreement with those of Shuford et al[36] who attribute the observed increases in the birefringence upon elongations, primarily to the changes in the degree of the preferred orientation of the crystalline phase. They[36] further argue that, as the draw ratio of the film is increased, the degree of orientation in the crystalline region and the corresponding changes in the observed birefringence reach

saturation values. The latter argument is supported by their observations with the sonic modulus[36] in stretched PVF_2 films. Hence the major contribution in the observed birefringence can be attributed to the orientation towards the stretch direction of the crystalline regions of PVF_2.

Figure 38 (SALS patterns) reveals the nature and mechanism of the orientation in which spherulitic distortion may play a major part. Figure 38(a) shows a typical H_v scattering pattern, prior to stretching with approximately 7^o scattering angle at the maximum lobe intensity. This type of four-lobe pattern, obtained with crossed polarizers, has been attributed to spherulite anisotropy.[21] The size of the spherulite may be calculated from such a four-lobe scattering pattern of undeformed spherulite using the following expression[21]

$$4\pi \frac{Ro}{\lambda} \text{Sin} \frac{\theta m}{2} = 4.1 \qquad \ldots\ldots \quad (2)$$

where Ro is the spherulite radius, the wavelength of the incident radiation, θm the angle for which the intensity of scattering is maximum. Using equation (2) the radius of the Form 2 spherulite in 50μm thick Kureha PVF_2 film, employed in the present work, was found to be ∿3μm.

It may be observed from figure 38 that as the draw ratio is increased the four-lobe scattering pattern changes into an eight-lobe scattering pattern, the uniaxial stretch being along the meridional direction. Following the quantitative investigations of spherulitic deformation upon elongation[37-40] Nomura et al[39,41,42] propose a model which takes into account rotation of crystallites as well as lamellar untwisting. In this model[42] they consider the existence of two types of crystal orientations within the lamellae of the undeformed spherulite, viz., type - 'R' in which the crystallites (and hence the principal optical axes) are randomly oriented and type - 'B' in which the optical axes preferentially lie at right angles to the spherulite radius (i.e.

b-axis radial orientation). The contribution to the light scattering intensity in the H_v mode due to type - 'R' crystal orientation may be neglected. They[42] further suggest (see figure 40) that the type - 'B' crystals may be subjected to two types of c-axis orientation, i.e. (i) due to crystal rotation around the a-axis associated with chain tilting (type - 'C_a') and (ii) due to unfolding of polymer chains (type - 'C_r'). The model predicts an alignment of c-axis in the stretch direction. The types - 'C_a' and 'C_r' crystals may be formed when the stretch direction is approximately parallel to the lamellar axis and lamellar untwisting will occur when the stretch direction is approximately perpendicular to the lamellar axis (figure 40) which is also in agreement with Yoon et al.[40] The computed theoretical SALS pattern[42] in the H_v mode shows that a four-lobe pattern, which must arise due to contribution from the type - 'B' crystal orientation only, for undeformed spherulites may give rise to an eight-lobe pattern on uniaxial stretching when re-orientations of the crystals, i.e. types - 'C_a' and 'C_r' are considered. With increasing stretch ratio the lamellar untwisting may begin to occur and this would extend the original four-leaf clover pattern in the meridional zone. Furthermore, the azimuthal angle μ figure 37) may begin to increase from the 45^o position and more progressively towards the equatorial zone with increasing stretch ratio. Subsequent to these two initial mechanisms of spherulite deformation, two other additional contributions may arise due to the formation of types 'C_a' and 'C_r' crystals (only at high values of stretch ratio) giving rise to eight or more lobes SALS pattern. The SALS patterns (figure 38) observed in the present work are in apparent agreement with Nomura et al[42] inasmuch that, on uniaxial stretching of PVF_2 films, an eight-lobe pattern is formed. Four of the lobes move progressively towards the equatorial zone (i.e. at right angles to the stretch direction), the remaining four lobes moving initially towards the stretch direction and

then increasing their azimuthal angle back to 45^{o} at approximately 90% stretch ratio. However, it may be observed (figure 38) that the scattering pattern changes into an eight-lobe type over a relatively small range of draw ratio (0 - 60%). This may not be satisfactorily explained by the model due to Nomura et al[42] which proposes a continuous change of orientation within a deforming spherulite upon elongation. A possible explanation for this observed behaviour of the scattering pattern at low elongation may be as follows. A structural transition from Form 2 to Form 1 in PVF_2 may occur on uniaxial stretching either at a discrete yield boundary within a spherulite, or by the growth of the new structure due to localised melting, for example, and a subsequent recrystallization, thus providing an orientation towards the stretch direction. The SALS pattern may then be expected to consist of an eight-lobe type profile superimposed with the scattering pattern of the recrystallized material which would be in evidence towards a position at right angles to the stretch direction for low elongation. It may be noted that no distinctive changes from the observed four-leaf SALS pattern (figure 38a) was observed on corona poling of unstretched PVF_2 film. Furthermore, there was no noticeable change of the eight-leaf SALS patterns (figure 38) on corona poling of the stretched films. These observations further confirm that, in contrast to the effect of uniaxial stretching, corona poling alone, even at very high fields ($3\times10^{8}Vm^{-1}$), does not produce a deformation of the spherulites.

References

1. Y. Wada and R. Hayakawa, Jap. J. Appl. Phys., 15(11), 2041 (1976).
2. J.B. Lando, H.G. Olf & A. Peterlin, J. Polym. Sci., A-1, 4, 941 (1966).
3. R. Hasegawa, Y. Takahashi, Y. Chatani & H. Tadokoro, Polym. J. 3(5), 600 (1972).
4. K. Nakamura & Y. Wada, J. Polym. Sci., A-2 9, 161 (1971).
5. R.G. Kepler & R.A. Anderson, J. Appl. Phys., 49(3), 1232 (1978).
6. N. Murayama, T. Oikawa, T. Katto & N. Nakamura, J. Polym. Sci., Polym. Phys. Ed., 13, 1033 (1975).
7. J. F. Nye, 'Physical Properties of Crystals', Oxford Univ. Press (1957) p.110.
8. H. Ohigashi, J. Appl. Phys., 47, 949 (1976).
9. M. Tamura, K. Ogasawara, N. Ono and S. Hagiwara, J. Appl. Phys., 45, 3768 (1974).
10. M. Oshiki and E. Fukada, J. Materials Sci., 10, 1 (1975).
11. P. Buchman, Ferroelectrics, 5, 39 (1973).
12. K. Ogasawara, K. Shiratori and M. Tamura, Rep. Prog. Polym. Phys. Japan, 19, 313 (1976).
13. M. Oshiki & E. Fukada, Jap. J. Appl. Phys., 15, 43 (1976).
14. Ye. L. Gal'perin, B. P. Kosmynin & V. K. Smirnov, Polymer Science (USSR) 12, 2133 (1970) Translated from Vysokol Soyed, A12 No. 8, 1880 (1970).
15. K. Nakagawa and Y. Ishida, Kolloid Z., 251, 103 (1973).
16. R. A. Creswell, M. M. Perlman & M. A. Kobayama, 'Dielectric Properties of Polymers', Ed. F. E. Karasz (Plenum., N.Y.), 295-312 (1972).
17. G. Pfister & M. A. Abkowitz, J. Appl. Phys., 45(3), 1001-1008 (1974).
18. E. J. Sharp & L. E. Garn, Appl. Phys. Lett., 29(8), 480 (1976).
19. R. L. Peterson, G. R. Day, P. M. Gruzensky & R. J. Phelan, Jr., J. Appl. Phys., 45(8), 3296 (1974).
20. H. Burkard and G. Pfister, J. Appl. Phys., 45(8), 3360 (1974).

References (cont.)

21. R.S. Stein and [illegible]. Rhodes, J. Appl. Phys. 31, 1873 (1960).

22. H.T. Jessop, Brit. J. Appl. Phys. 4, 138 (1953).

23. D.K. Das Gupta & K. Doughty, Appl. Phys. Lett., 31(9), 585 (1977).

24. D.K. Das-Gupta & K. Doughty, to be published in J. Appl. Phys.

25. R.S. Brockley and D.B. Shier, UCNW Bangor (Private Communication) (1978).

26. B.L. Farmer, A.J. Hopfinger & J.B. Lando, J. Appl. Phys. 43(11), 4293 (1972).

27. G.T. Davis, J. E. JcKinney, M.G. Broadhurst & S.C. Roth, submitted to J. Appl. Phys. (Private communication).

28. G. Pfister, M. Abkowitz and R.G. Crystal, J. Appl. Phys. 44(5), 2064 (1973).

29. G.F.J. Garlick & A.F. Gibson, Proc. Phys. Soc. A, (London), 60, 574 (1948).

30. M.E. Lines & A.M. Glass, 'Principles and Applications of Ferroelectrics and Related Materials', (Clarendon Press, Oxford), 558 (1977).

31. R.G. Kepler, E. J. Graeber, & P.M. Beeson, Bull. Amer. Phys. Soc., Ser. 2, 20, 350 (1975).

32. S. Kavesh & J.M. Shultz, J. Polym. Sci., A-2, 8, 243 (1970).

33. M. Tamura, S. Hagiwara, S. Matsumoto & N. Ono, J. Appl. Phys. 48(2), 513 (1977).

34. N. Murayama & H. Hashizumi, J. Polym. Sci., Polym. Phys. Ed., 14, 989 (1976).

35. V. Petraccone, I.C. Sanchez & R.S. Stein, J. Polym. Sci., Polym. Phys. Ed., 13, 1991 (1975).

36. R.J. Shuford, A.F. Wilde, J.J. Ricca & G.R. Thomas, Polym. Eng. Sci., 16(1), 25 (1976).

37. K. Sasaguri, S. Hosino & R.S. Stein, J. Appl. Phys. 35(1), 47 (1964).

38. S. Clough, J.J. Van Aartsen & R.S. Stein, J. Appl. Phys. 36(10), 3072 (1965).

39. N. Nomura, A. Asanuma, S. Suehiro & H. Kawai, J. Polym. Sci. A-2, 9, 1991 (1971).

References (cont.)

40. D.Y. Yoon, C. Chang & R.S. Stein, J. Polym. Sci., Polym. Phys. Ed., 12, 2091 (1974).

41. S. Nomura, M. Matsuo & H. Kawai, J. Polym. Sci., Polym. Phys. Ed., 10, 2489 (1972).

42. S. Nomura, M. Matsuo & H. Kawai, J. Polym. Sci., Polym. Phys. Ed., 12, 1371 (1974).

Legends

Fig. 1: Form 1 PVF_2 viewed along c-axis (along main chains).

Fig. 2: Form 2 PVF_2 viewed along c-axis (along main chains).

Fig. 3: Separation of X-ray diffraction profile of 50μm thick PVF_2, containing crystallites only of Form 2, into crystalline and amorphous contributions and to estimate crystallinity by the method due to Gal'perin (1970).

Fig. 4: Crystallinity of Form 2 PVF_2 at various temperatures.

Fig. 5: X-ray diffraction peaks of Form 2 PVF_2 at different temperatures.

Fig. 6: Thermal expansion of Form 2 PVF_2 (from X-ray diffraction profiles of 50μm sample).

Fig. 7: X-ray diffraction patterns of (50μm) PVF_2 corona poled at 20°C (unstretched).

Fig. 8: Diffraction peak heights vs. surface potential for Form 2 sample (50μm thick).

Fig. 9: Corona induced changes in higher order peaks for Form 2 sample (50μm thick).

Fig. 10: Corona induced changes in higher order peaks for Form 2 sample (50μm thick).

Fig. 11: Changes in X-ray diffraction pattern of Form 2 PVF_2 corona charged to breakdown potential (18KV) at 20°C (50μm thick).

Fig. 12: X-ray diffraction patterns of Form 2 PVF_2 charged to 10KV (50μm thick).

Fig. 13: Corona charging of Form 2 PVF_2 at -80°C for 60s with 10KV (50μm thick).

Fig. 14: Behaviour of d_{31} of Form 2 PVF_2 (50μm thick) with corona charging to high surface potentials at various temperatures.

Fig. 15: Piezoelectric activity vs. log charging time for Form 2 PVF_2 PVF_2 (50μm thick).

Legends (cont.)

Fig. 16: X-ray diffraction patterns as a function of the poling (corona charging) field; (25μm thick PVF_2 film, Form 1 + Form 2)

Fig. 17: Effect of increasing field on higher order peaks of samples originally containing Form 1 and Form 2; Bragg angles 25° - 34° (2θ).

Fig. 18: Effect of increasing field on higher order peaks of samples originally containing Form 1 and Form 2; Bragg angles 35° - 38° (2θ).

Fig. 19: Peak intensities of major peaks of 25μm thick PVF_2, corona charged at $20^{\circ}C$ for 30 minutes.

Fig. 20: Major peak intensities vs. surface potential for samples containing Form 1 and Form 2 corona charged for 60 seconds at $100^{\circ}C$.

Fig. 21: Comparison of thermal expansion in Form 1 and Form 2 PVF_2.

Fig. 22: Piezoelectricity against corona charging time for a surface potential of 7.5KV.

Fig. 23: Piezoelectricity vs. poling temperatures for different corona poling fields; (Poling time 5 minutes : 25μm thick PVF_2).

Fig. 24: Comparison of piezoelectric activity due to positive and negative corona (25μm thick PVF_2).

Fig. 25: Piezoelectric responses with different electrode materials (aluminium, gold and silver dag) in corona charged 25μm thick PVF_2 films.

Fig. 26: Effect on piezoelectricity of cooling a charged sample to ambient temperature before removing the corona charging; (25μm thick PVF_2).

Fig. 27: X-ray diffraction patterns of 50μm PVF_2 stretched and corona charged.

Fig. 28: Corona charging of PVF_2 stretched 5 : 1 at $145^{\circ}C$.

Legends (cont.)

Fig. 29: Effect of breakdown potentials at 20°C on sample stretched 5 : 1 at 145°C; (22.5μm thick PVF_2).

Fig. 30: Piezoelectric strain coefficient d_{31} of corona charged PVF_2 with different stretch ratio; (50μm thick PVF_2).

Fig. 31: Piezoelectric activity of stretched and corona charged PVF_2 stretched 5 : 1 at 145°C; (Form 1 and Form 2 mixture).

Fig. 32: Piezoelectric activity of Form 1 PVF_2 – conventional poling ; sample stretched 5 : 1 at 110°C.

Fig. 33: Piezoelectric activity of corona charged Form 1 PVF_2; sample stretched 5 : 1 at 110°C.

Fig. 34: Thermally stimulated current (TSC) during the first heating cycle (irreversible) in corona charged PVF_2 film of 25μm thickness.
A : Corona potential 10KV; charging time 100s at 20°C.
B : Corona potential 5KV; otherwise as in A.

Fig. 35: The behaviour of the (reversible) piezoelectric strain coefficient d_{31} of corona charged PVF_2 film of 25μm thickness. Poling conditions for curves A and B are the same as in figure 34.

Fig. 36: The experimental arrangement to obtain light scattering patterns in the H_v mode (crossed polarizers); 50μm thick PVF_2.

Fig. 37: Birefringence of PVF_2 (originally 50μm thick) with different stretch ratios.

Fig. 38: Small angle light scattering (SALS) patterns of PVF_2 with different stretch ratios. a, b, c, d, e and f represent no stretch, 10%, 30%. 60%, 95% and 140% stretch ratios respectively.

Fig. 39: Suggested intermediate form after corona charging.

Fig. 40: Processes of spherulite deformations on uniaxial stretching.

Program of Work for the period

September 1978 - August 1979

1. Continuation of studies of absorption currents and steady state conductivity in conventionally poled PVF_2.
2. Continuation of a study of ageing of stretched and corona poled PVF_2.
3. A study of X-ray pole figures in the presence of corona field.
4. Study of crystallinity changes with temperature and their effects on d_{31} and p.
5. Infrared spectral studies including attenuated total reflection (ATR) of corona charged PVF_2.

Proposed Program of Work for the period

September 1979 - August 1980

1. Complete dielectric characterization (i.e. behaviour of ε'') of corona poled PVF_2 and PVF films in the frequency range 10^{-5} to 10^{5}Ez.
2. A feasibility study of developing a technique for continuous corona poling of PVF_2 films.
3. A study of piezo- and pyroelectricity of γ-radiated and corona poled PVF_2.
4. Photo injected and thermally stimulated current PITSC) in PVF_2 before and after poling and with/without dc bias fields.

Form I PVF_2 viewed along c-axis (along main chains).
Figure 1.

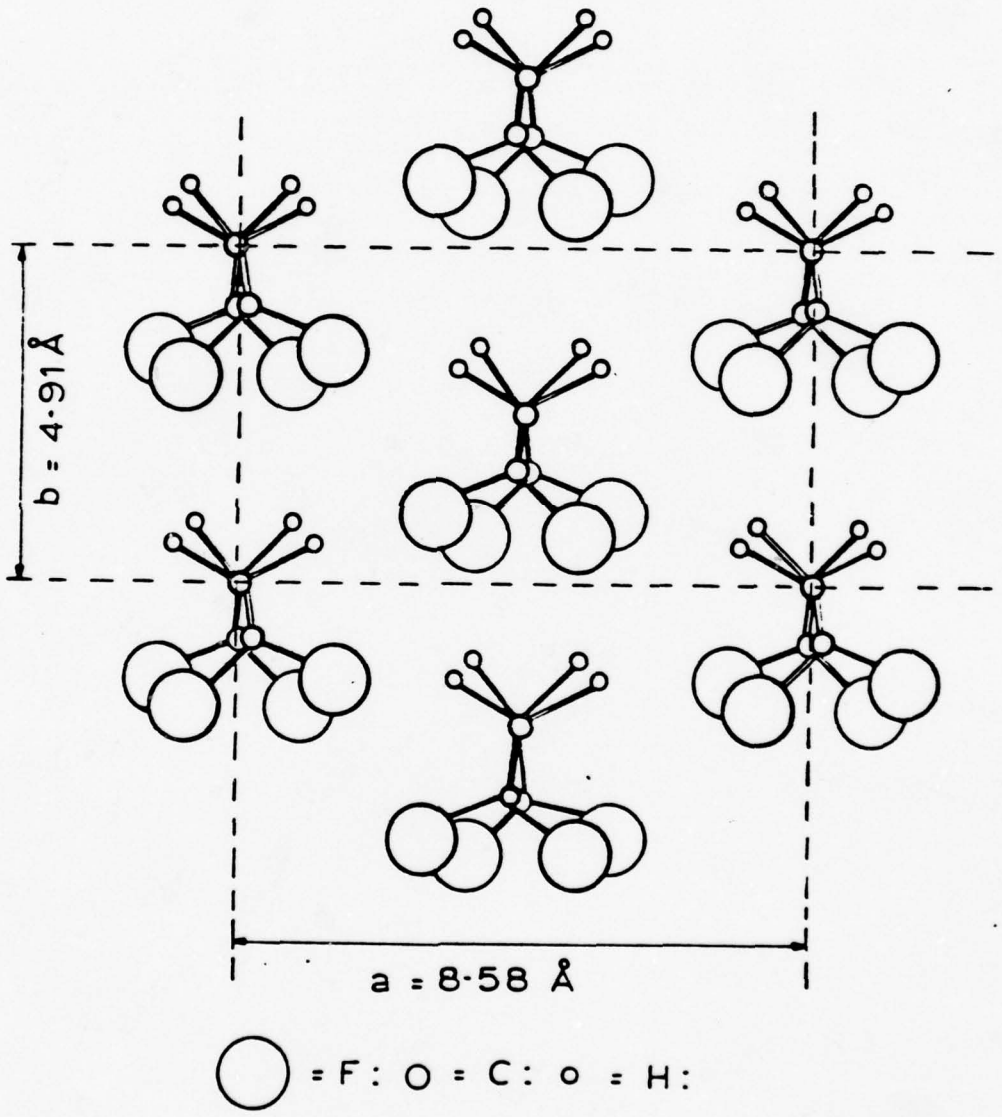

Form II PVF_2 viewed along c-axis (along main chains)
Figure 2.

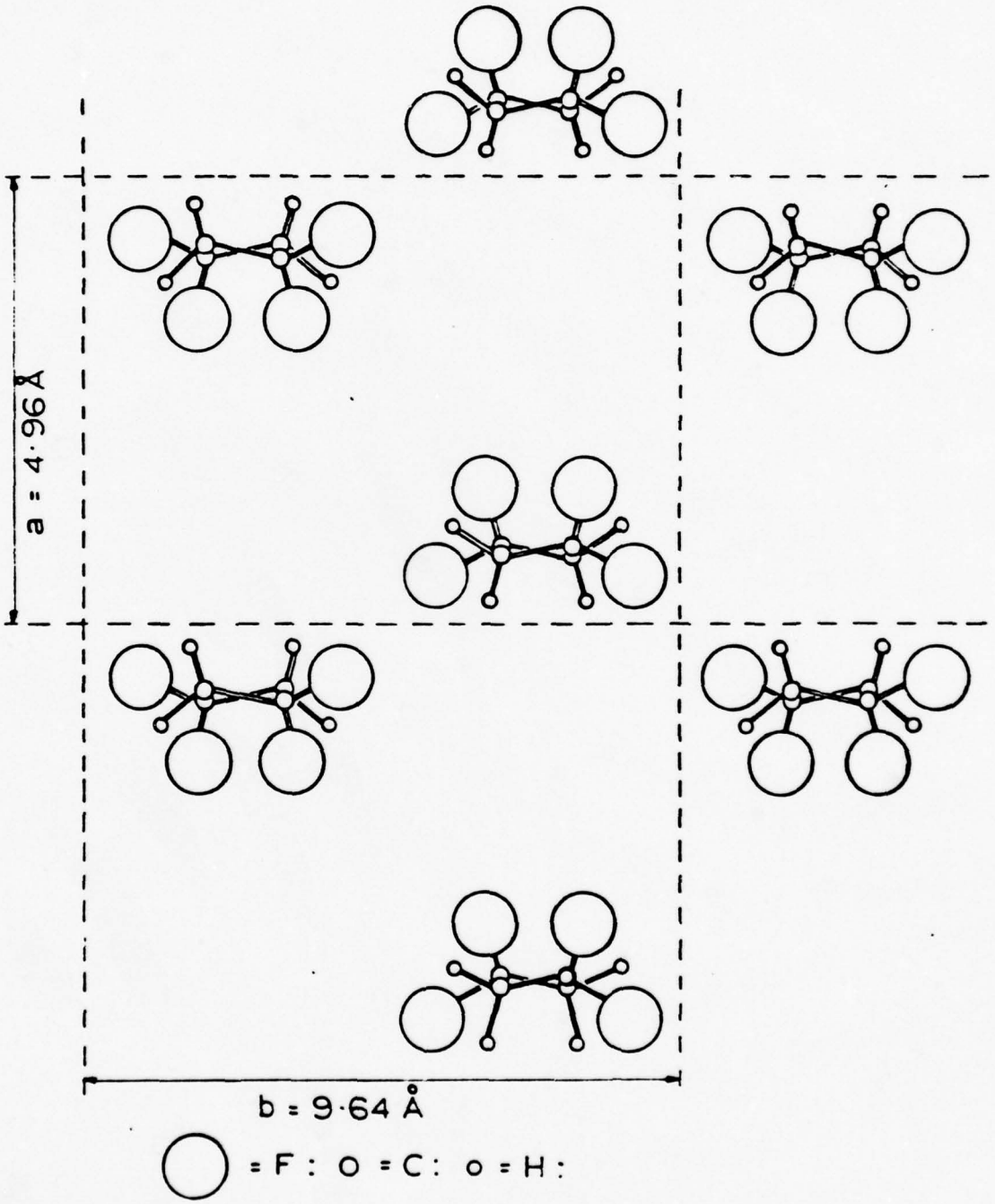

Figure 3:

Separation of X-ray Diffraction Profile of 50μm thick PVF_2, containing Crystallites only of Form 2, into Crystalline and Amorphous Contributions and to estimate Crystallinity by the method due to Gal'perin (1970)

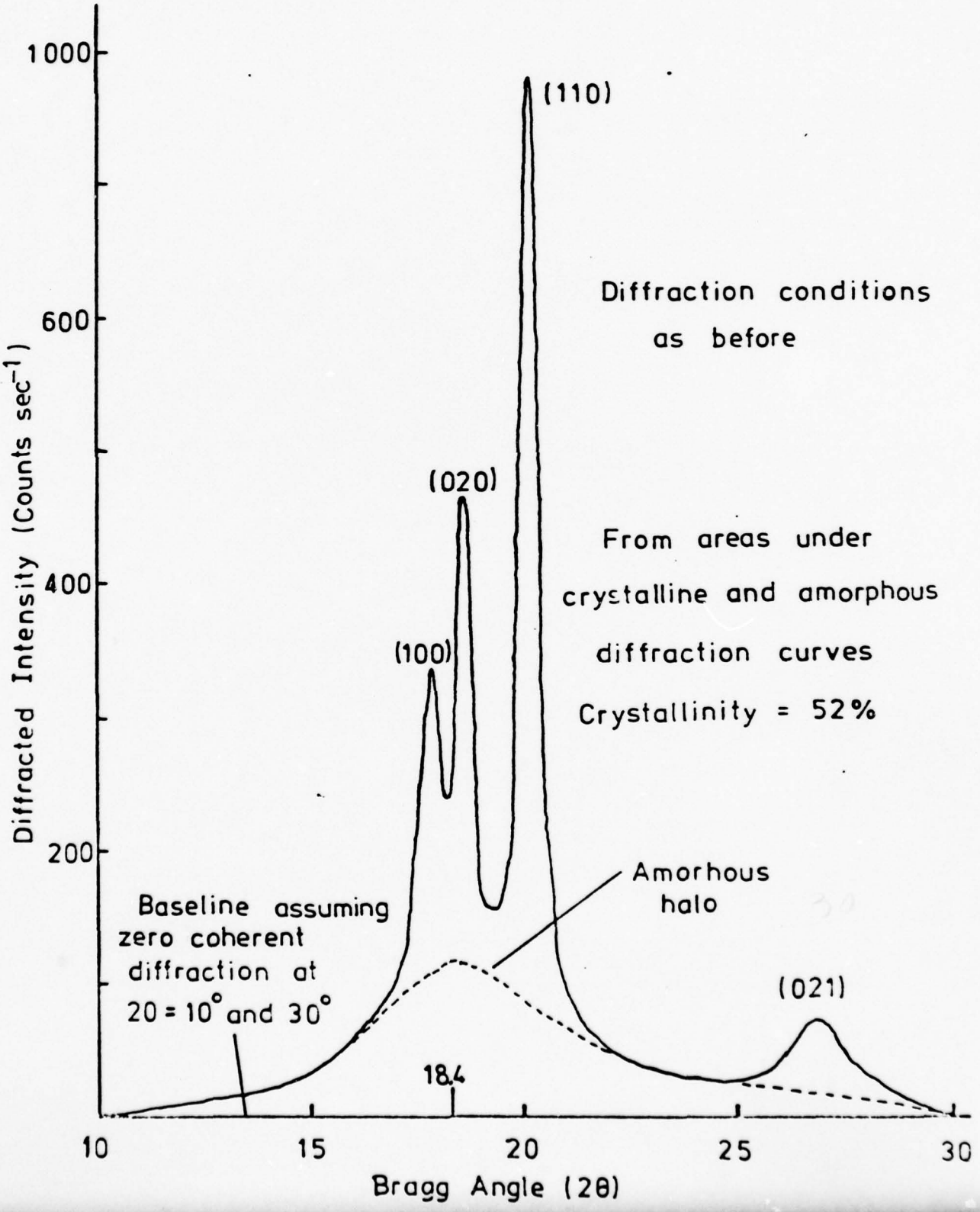

Figure 4:

Crystallinity of Form 2 PVF_2 at Various Temperatures

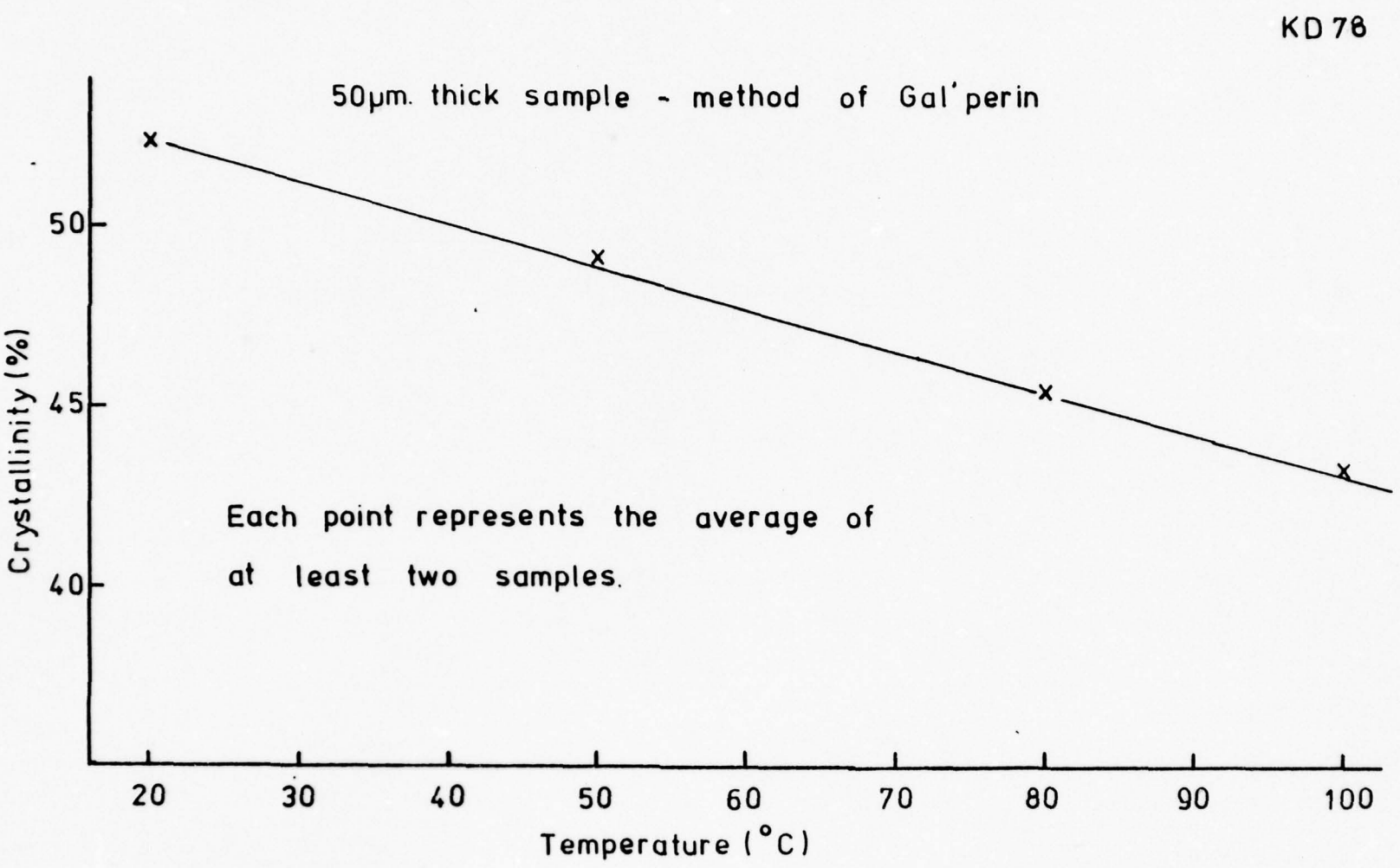

Figure 5:

X-Ray Diffraction Peaks of Form 2 PVF_2 at Different Temperatures

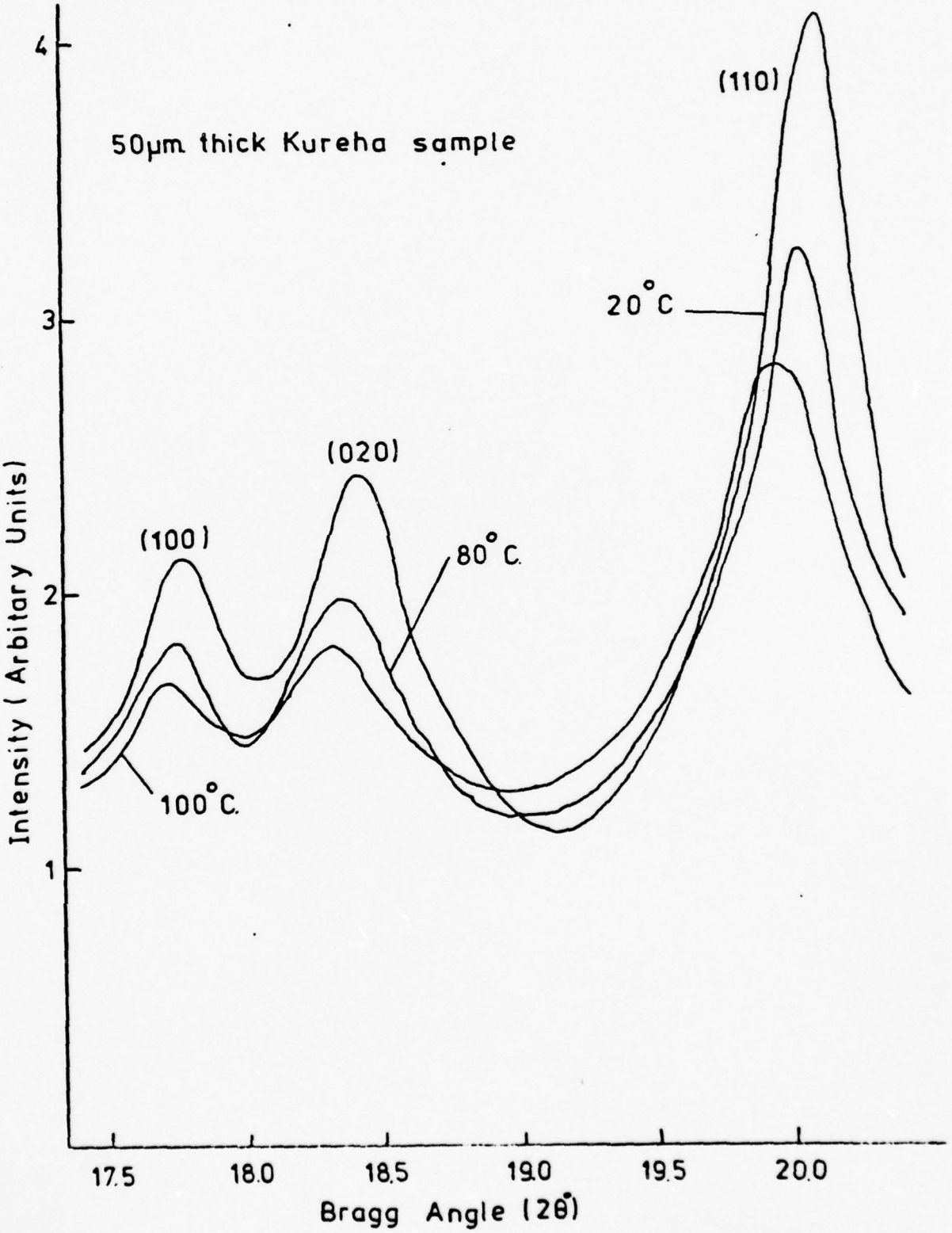

Figure 6:

Thermal Expansion of Form 2 PVF_2

(from x-ray diffraction profiles of 50μm. sample)

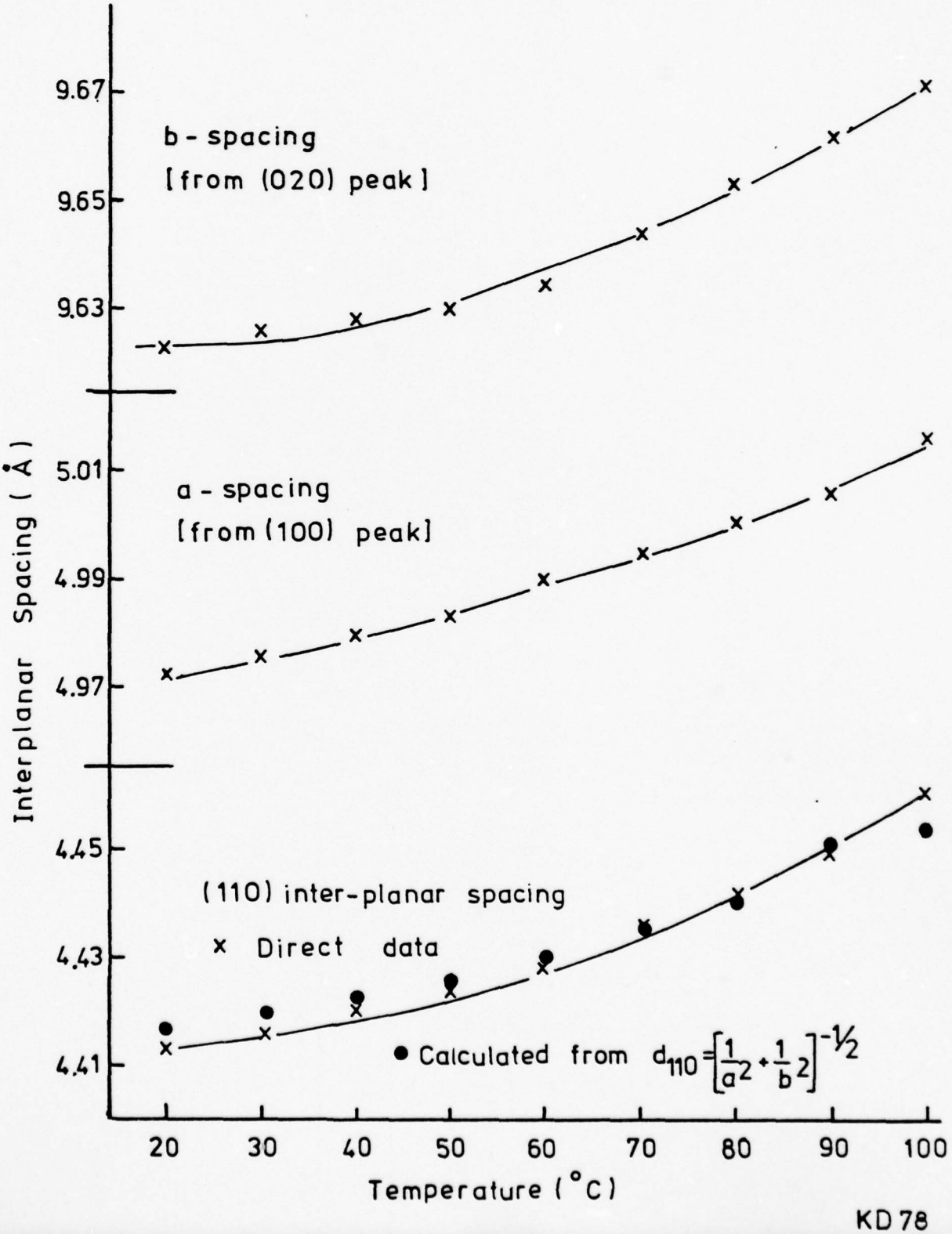

Figure 7:

X-Ray diffraction patterns of (50μm) PVF_2 poled at 20° C. (unstretched).

Figure

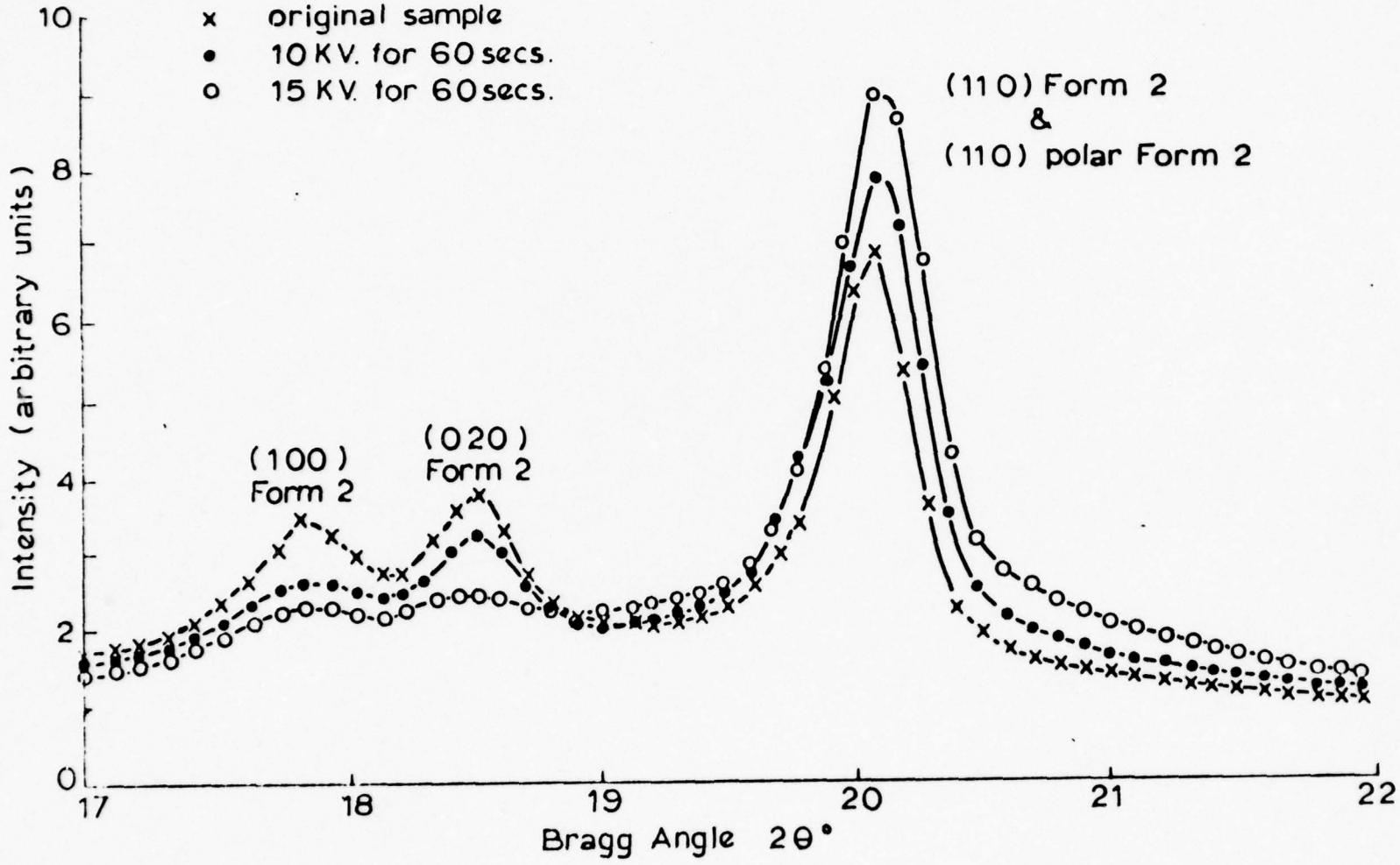

Figure 8:

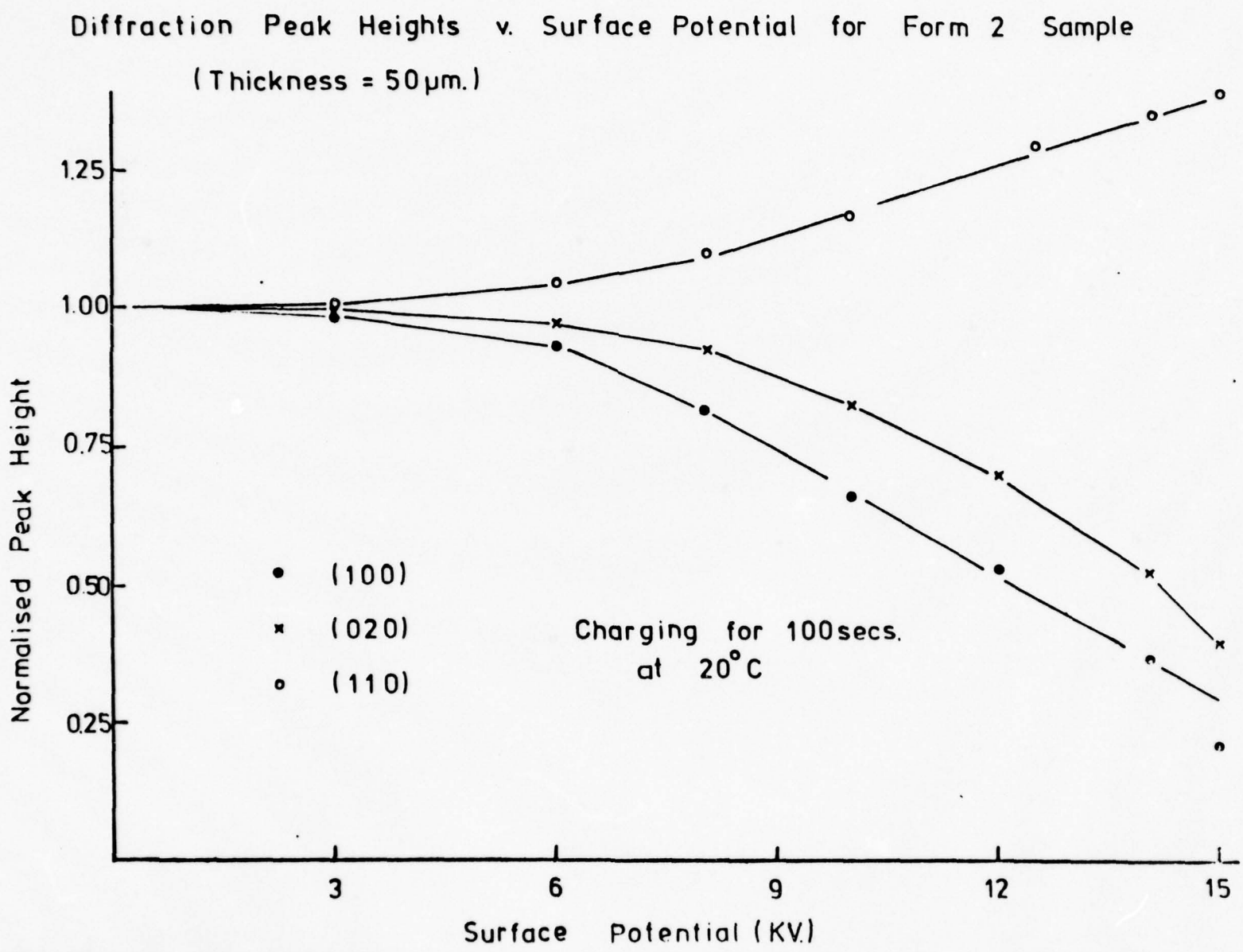
Diffraction Peak Heights v. Surface Potential for Form 2 Sample
(Thickness = 50μm.)
Normalised Peak Height
1.25
1.00
0.75
0.50
0.25
(100)
(020)
(110)
Charging for 100secs.
at 20°C
3
6
9
12
15
Surface Potential (KV.)

Figure 9:

Corona Induced Changes in Higher Order Peaks for Form 2 Sample (50μm. thick)

1. Bragg Angles 25° - 34° (2θ)

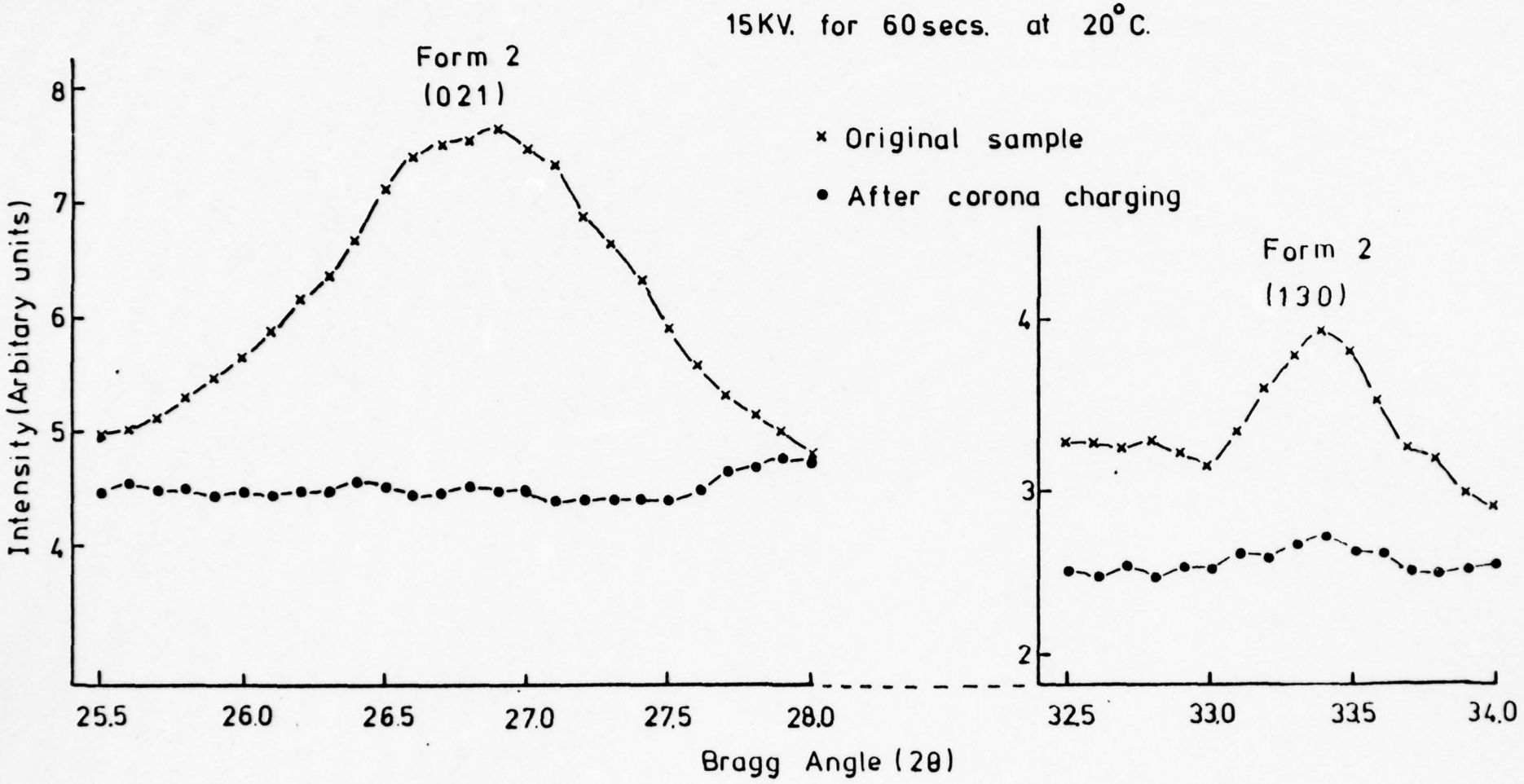

Figure 10:

Corona Induced Changes in Higher Order Peaks for Form 2 Sample (50μm. thick)

2. Bragg Angles $34^{\circ} - 40^{\circ}$ (2θ)

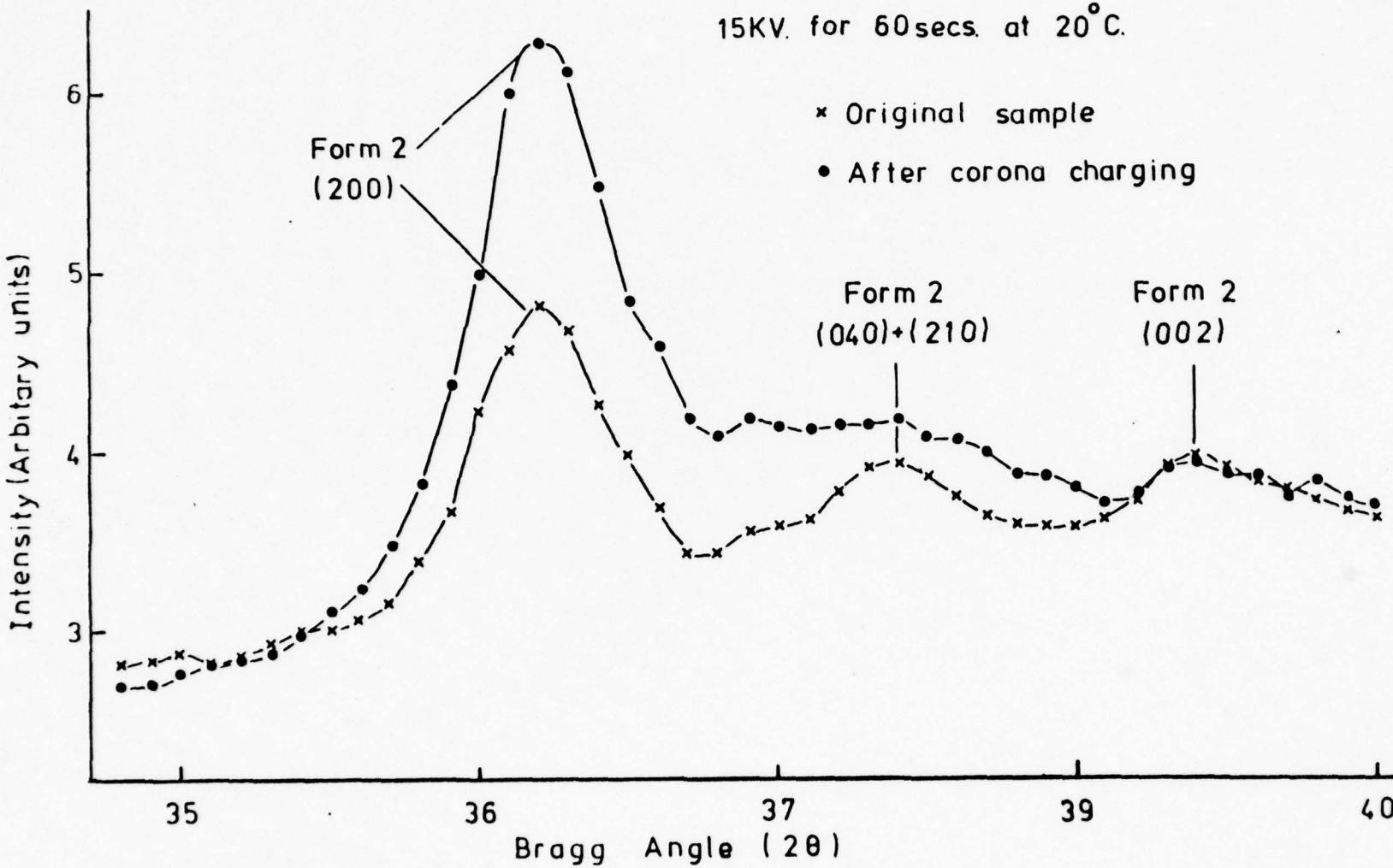

Figure 11:

Changes in X-Ray Diffraction Pattern of Form 2 PVF_2 Corona Charged to Breakdown Potential (18KV.) at 20°C. Sample thickness = 50μm.

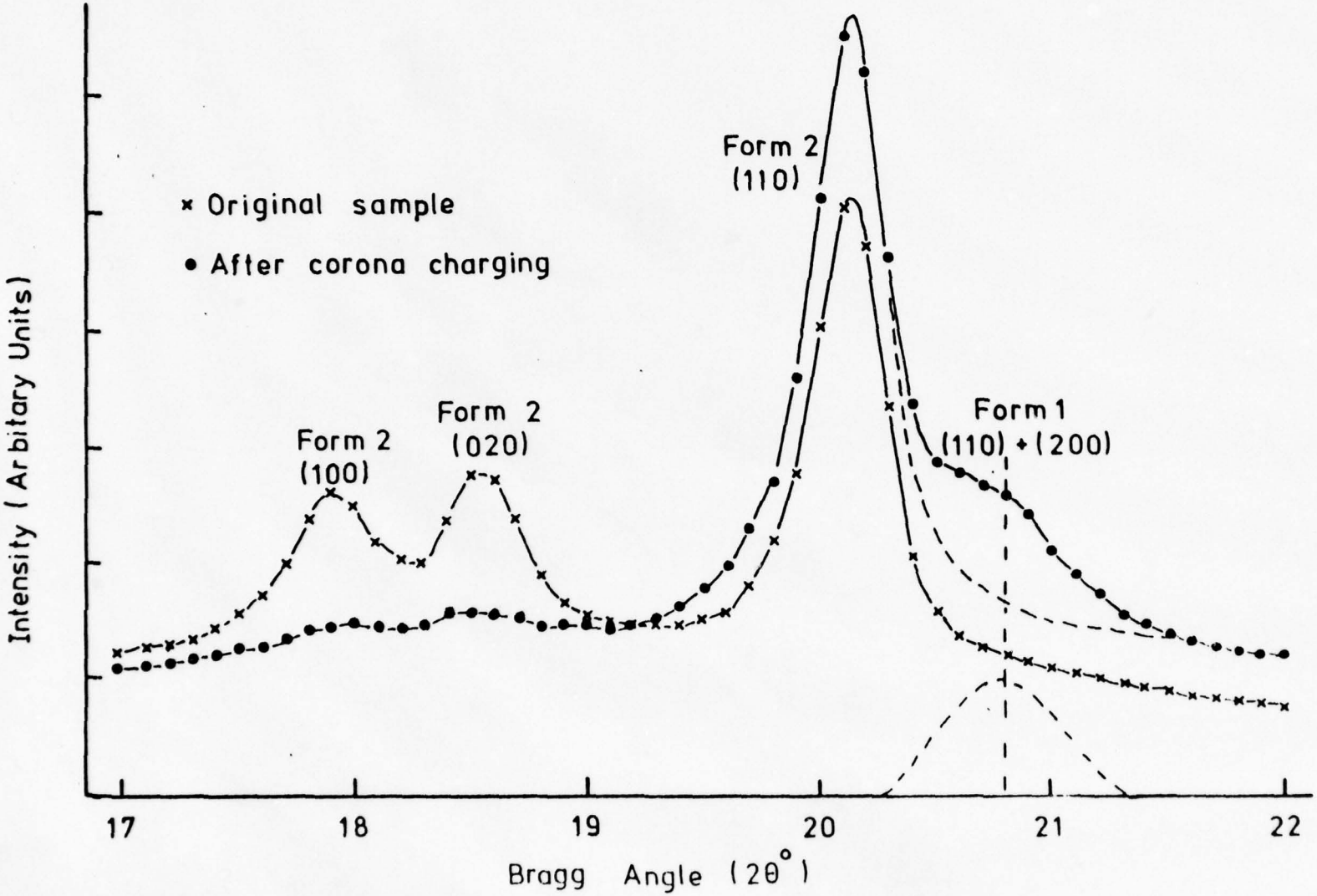

Figure 12:

X - Ray Diffraction Patterns of Form 2 PVF_2 Charged to 10KV.

Sample thickness = 50 μm.

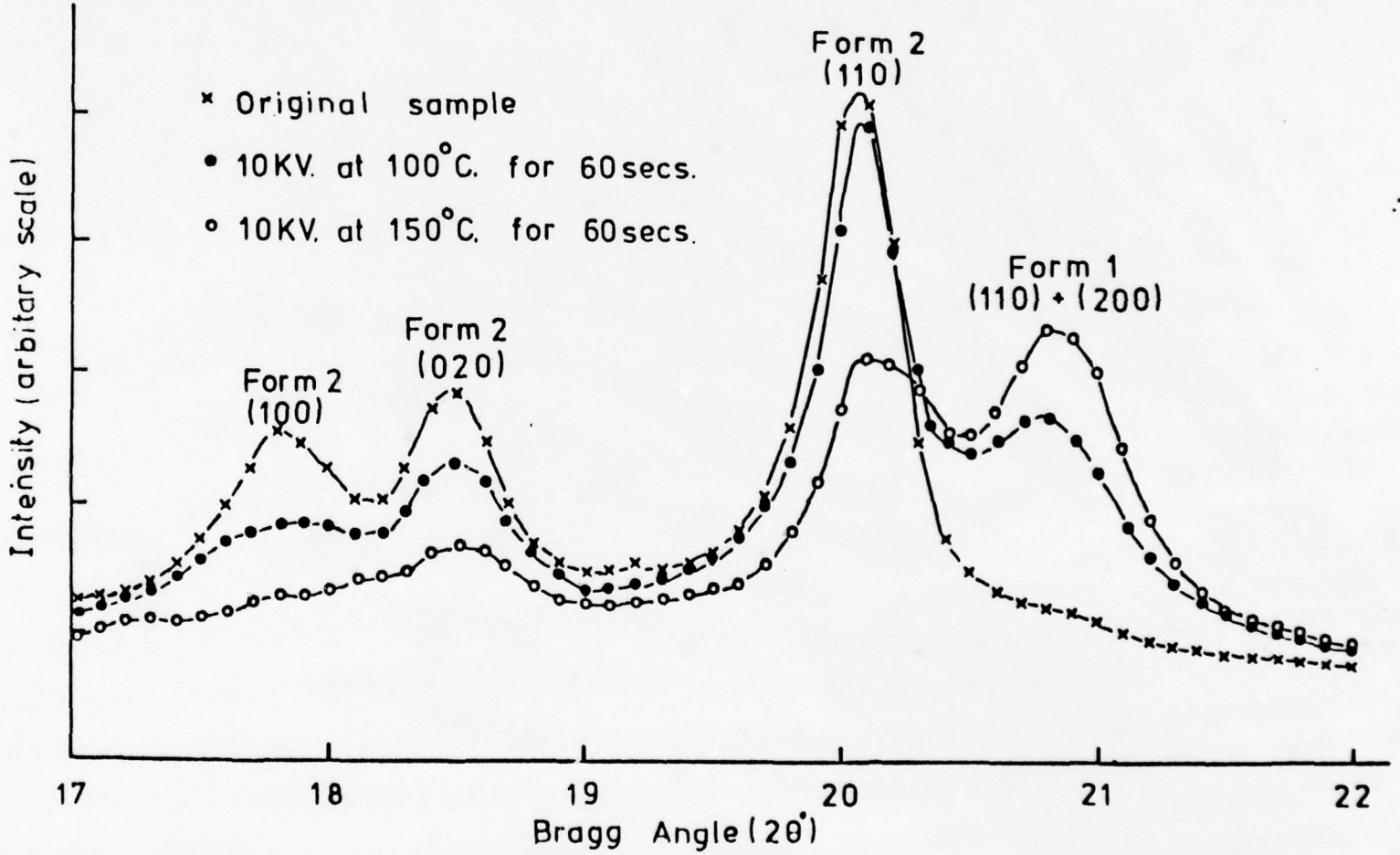

Figure 13:

Corona Charging of Form 2 PVF_2 at -80°C for 60secs with 10KV.

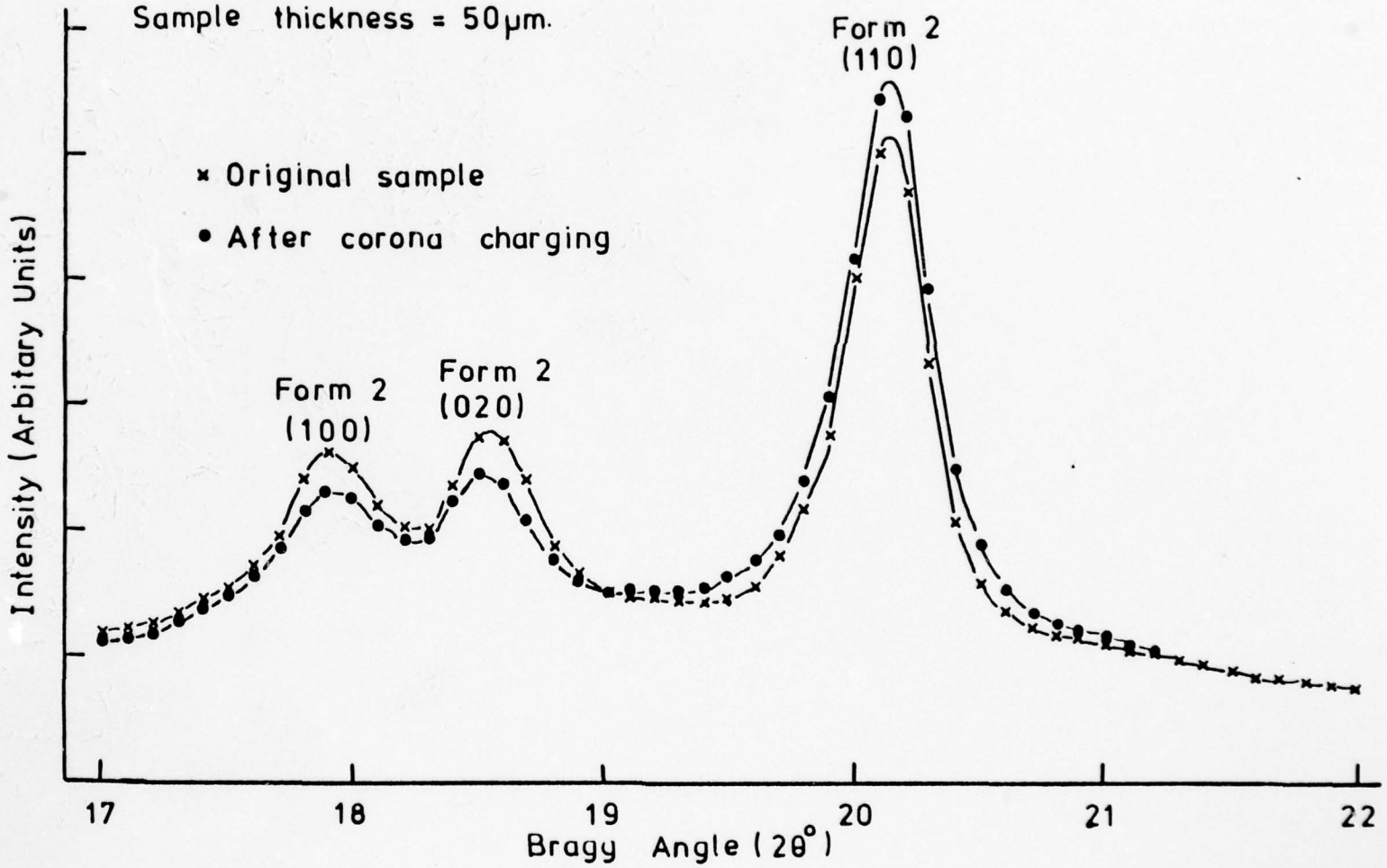

Figure 14:

Behaviour of d_{31} of Form 2 PVF_2 (50μm. thick) with Corona Charging to High Surface Potentials at Various Temperatures

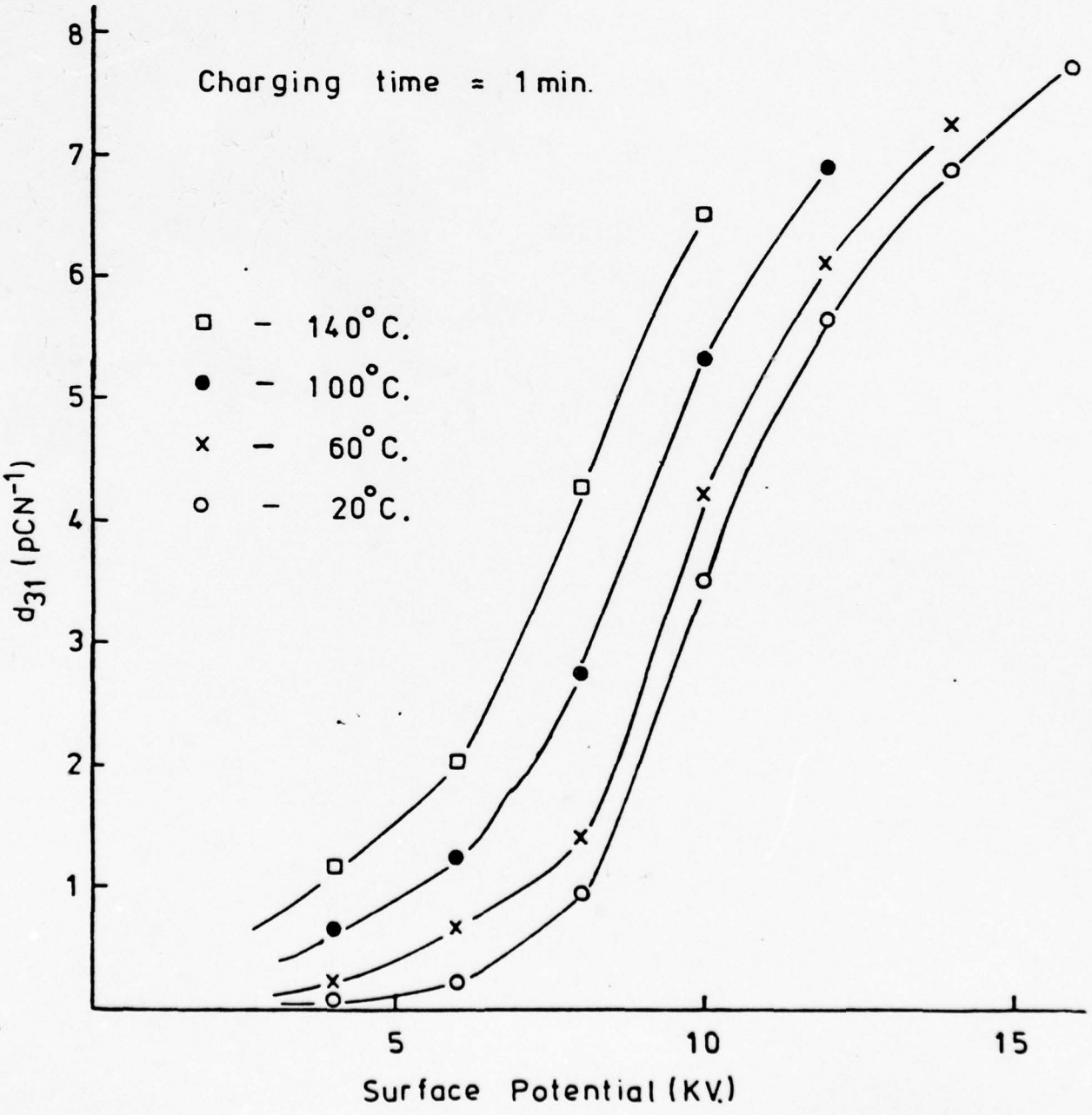

Figure 15:

Piezoelectric Activity vs. Log. Charging Time for Form 2 PVF_2 (50μm thick)

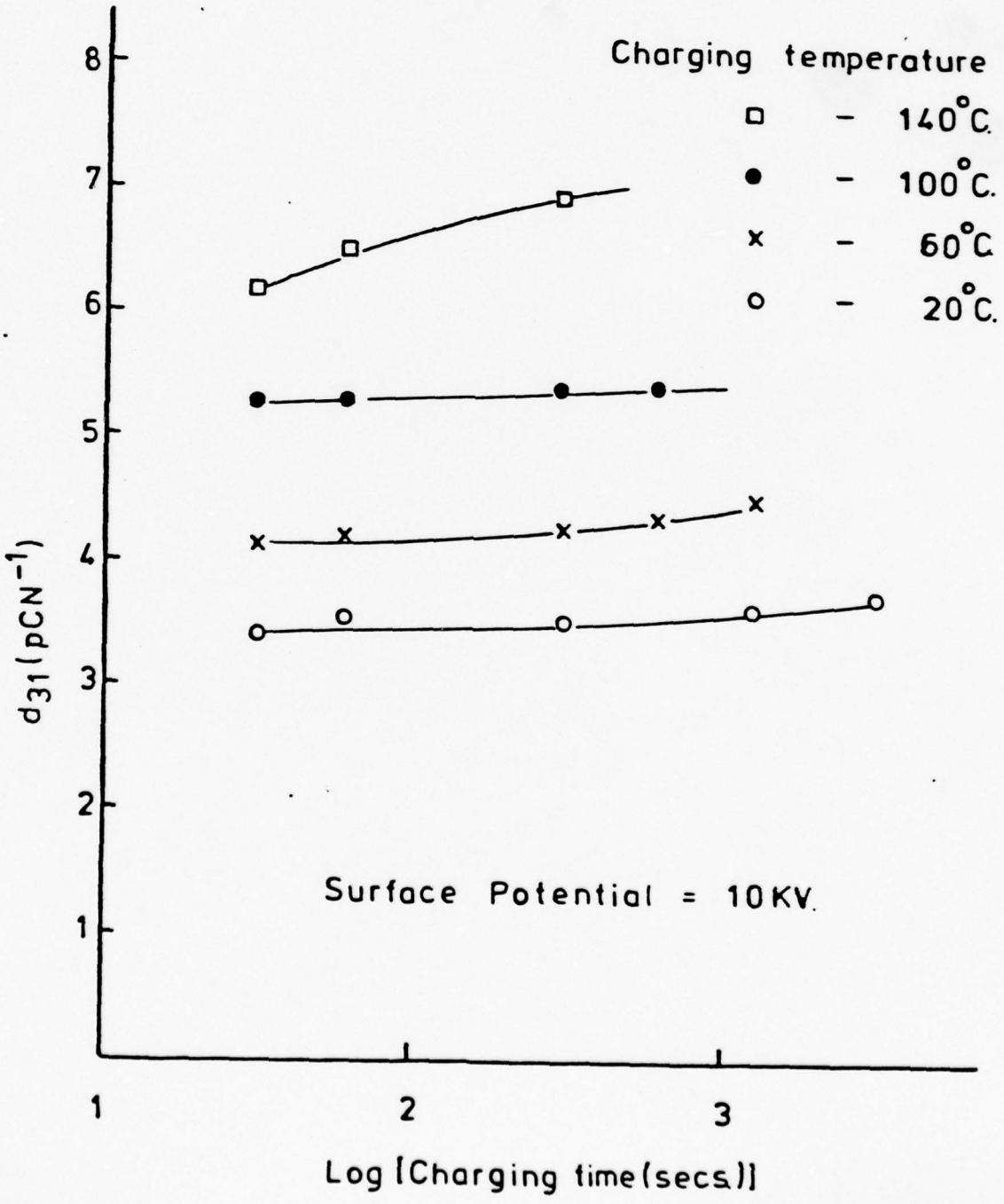

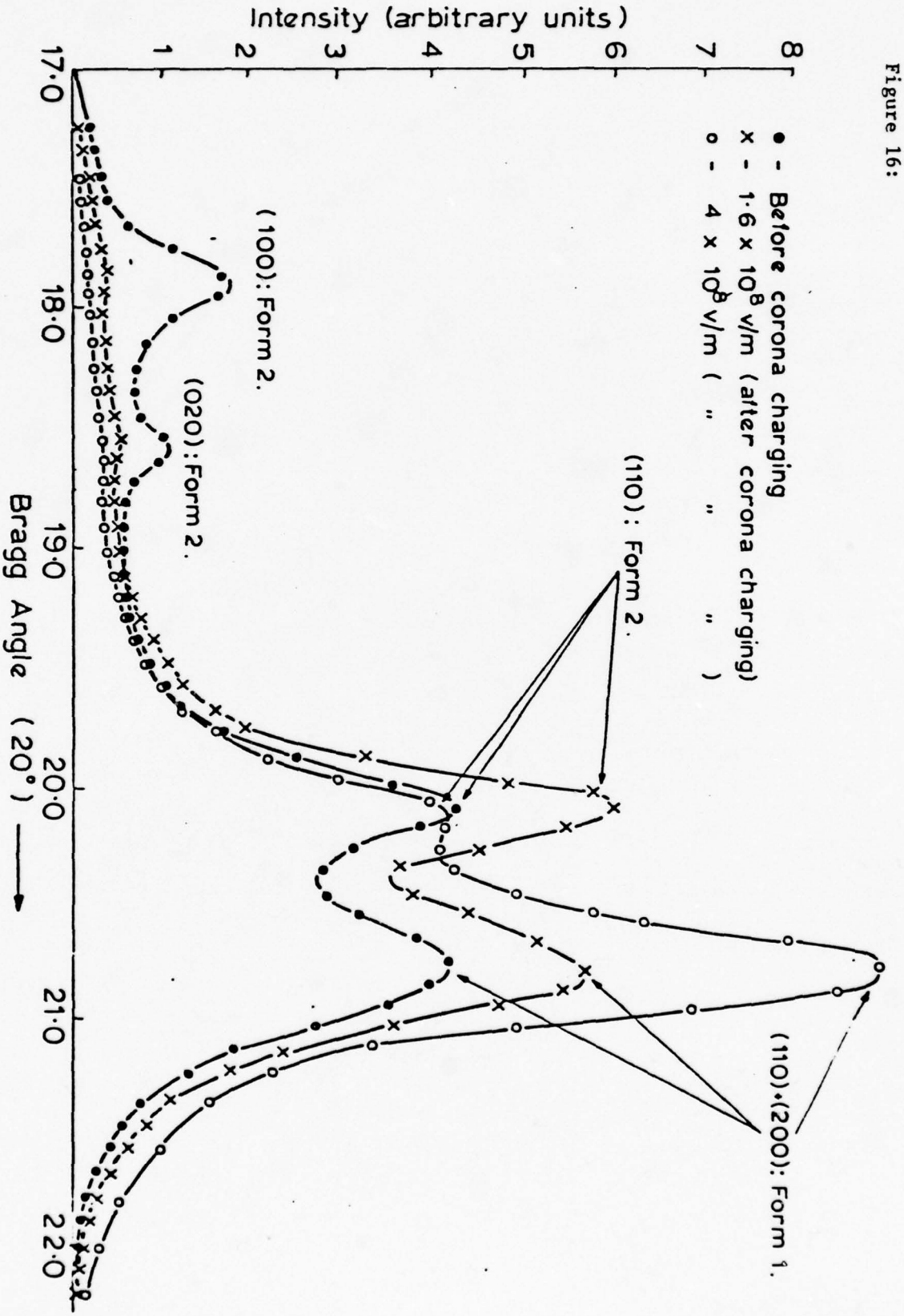
Intensity (arbitrary units)
1
2
3
4
5
6
7
8
17·0
18·0
19·0
20·0
21·0
22·0
Bragg Angle (2θ°) ⟶
● - Before corona charging
× - 1·6 × 10⁸ v/m (after corona charging)
o - 4 × 10⁸ v/m (" " ")
(100): Form 2.
(020): Form 2.
(110): Form 2.
(110)+(200): Form 1.

Figure 16:

Figure 17:

Effect of Increasing Field on Higher Order Peaks of Samples Originally Containing Form 1 and Form 2. 1 - Bragg Angles $25^{\circ} - 34^{\circ}$ (2θ)

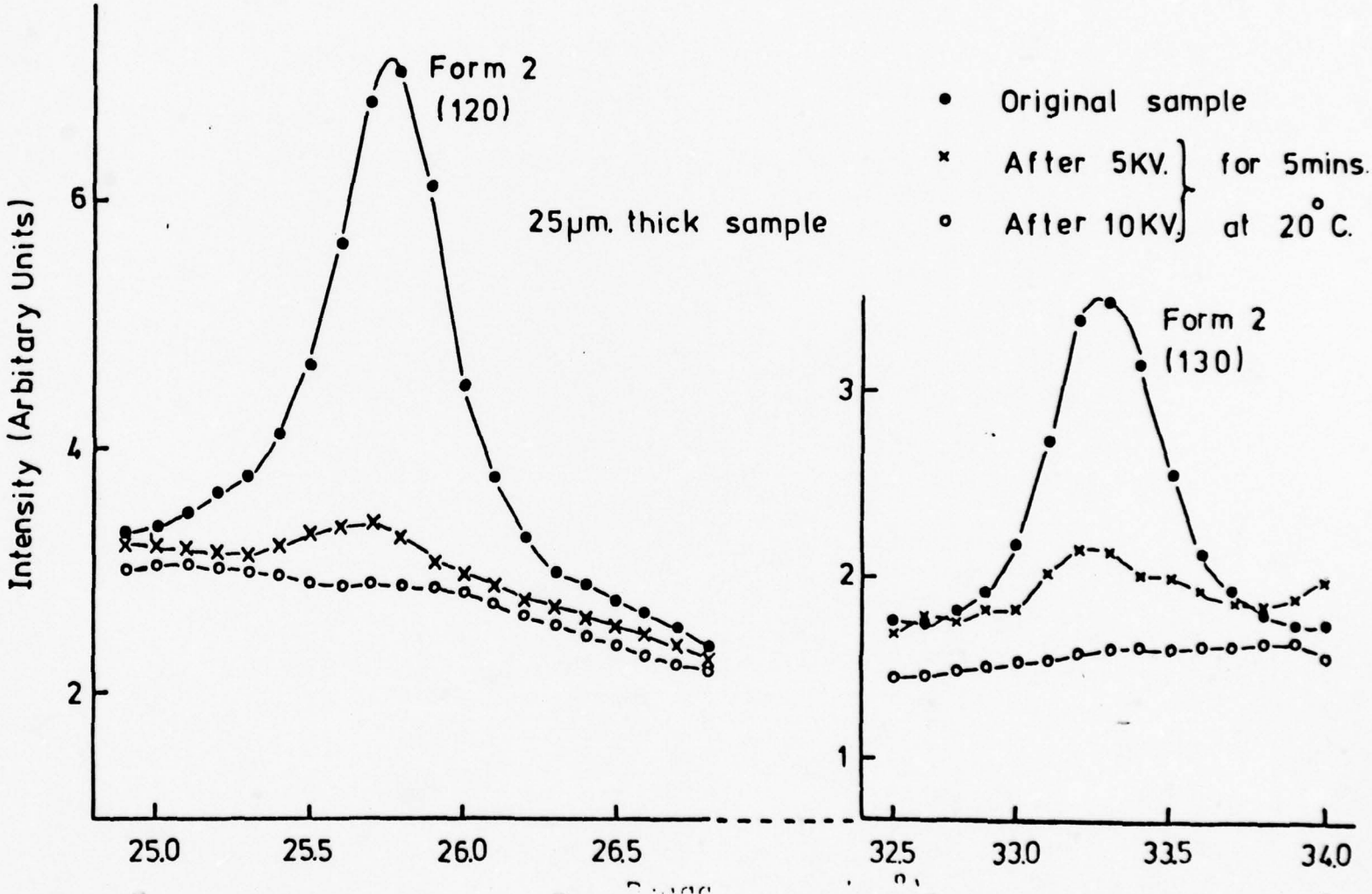

Figure 18:

Effect of Increasing Field on Higher Order Peaks of Samples Originally Containing Form 1 and Form 2

2 - Bragg Angles $35^{\circ} - 38^{\circ}$ (2θ)

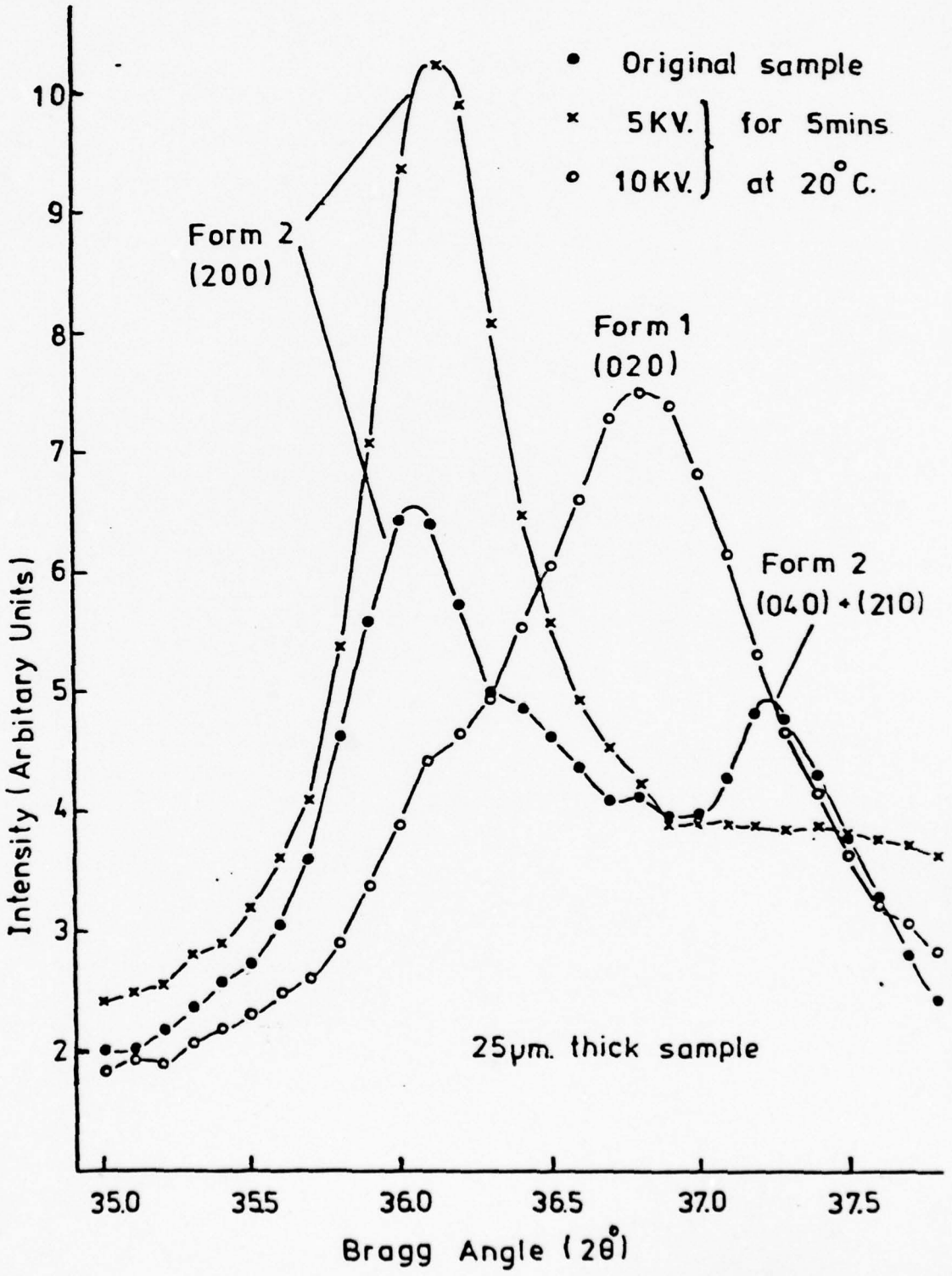

Figure 19:

Peak Intensities of Major Peaks of 25μm. Thick Sample Corona Charged at 20°C. for 30mins.

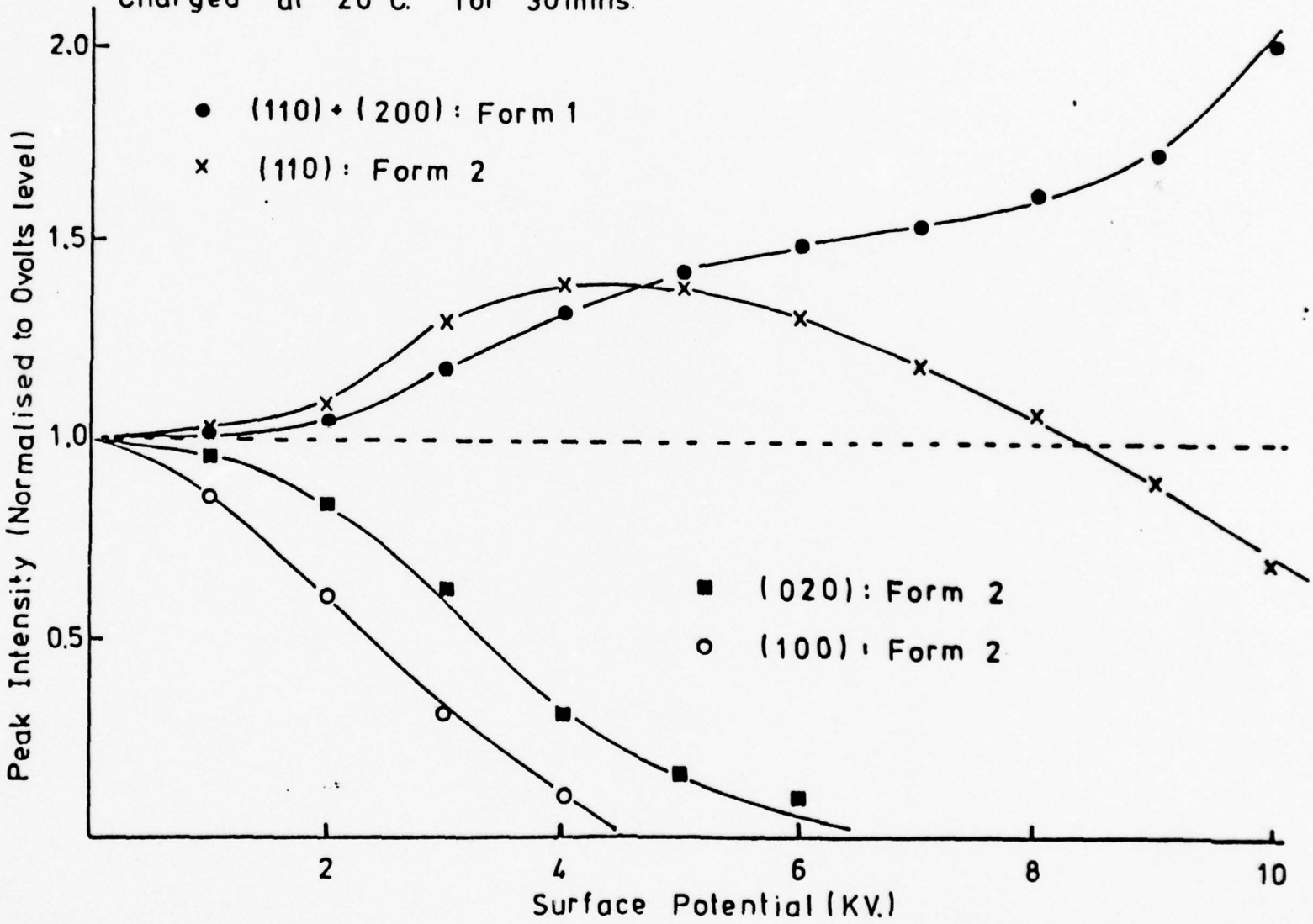

Figure 20:

Major Peak Intensities v. Surface Potential for Samples Containing Form 1 and Form 2 Corona Charged for 60secs. at 100°C.

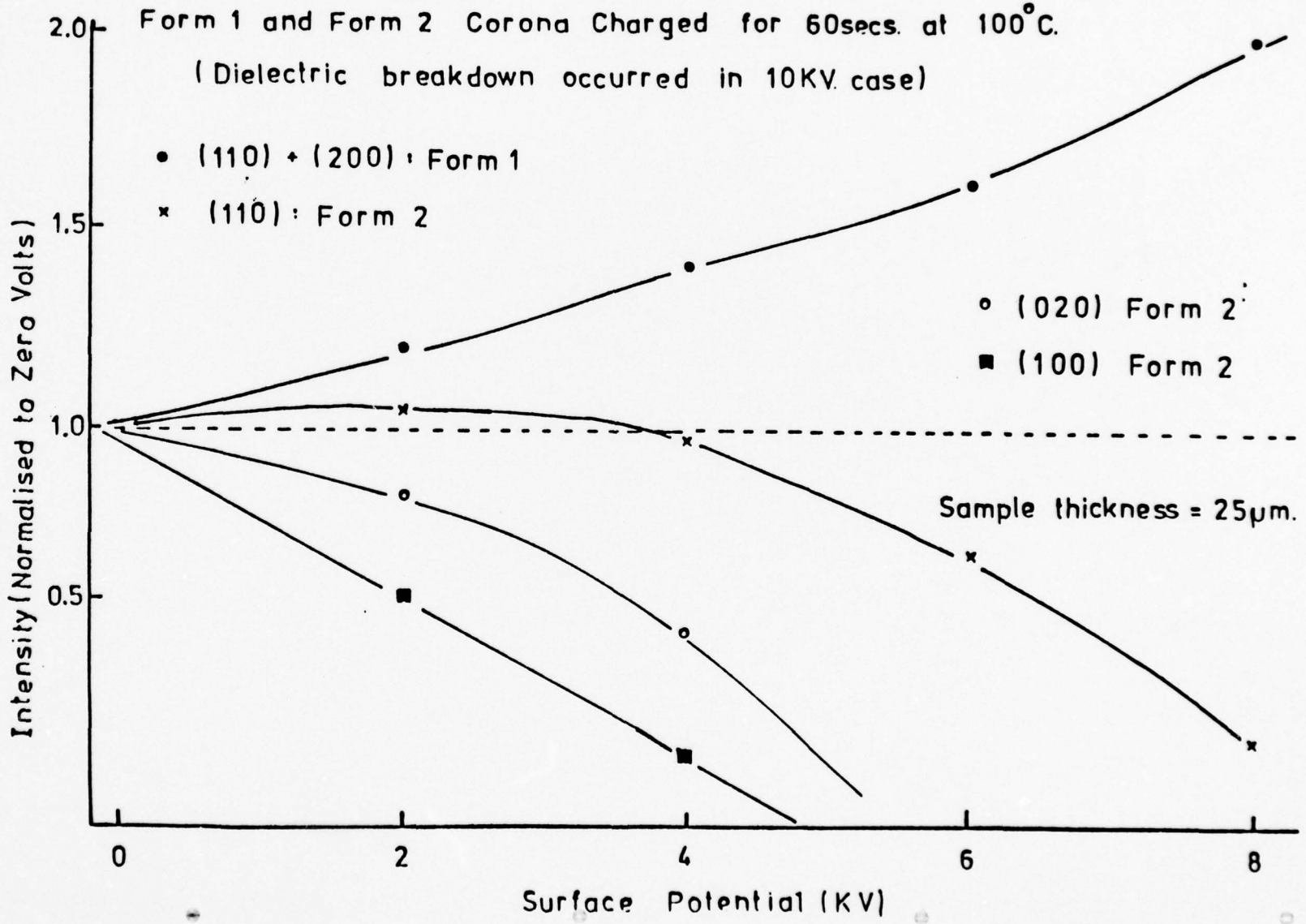

Figure 21:

Comparison of Thermal Expansion in Form 1 and Form 2 PVF_2.

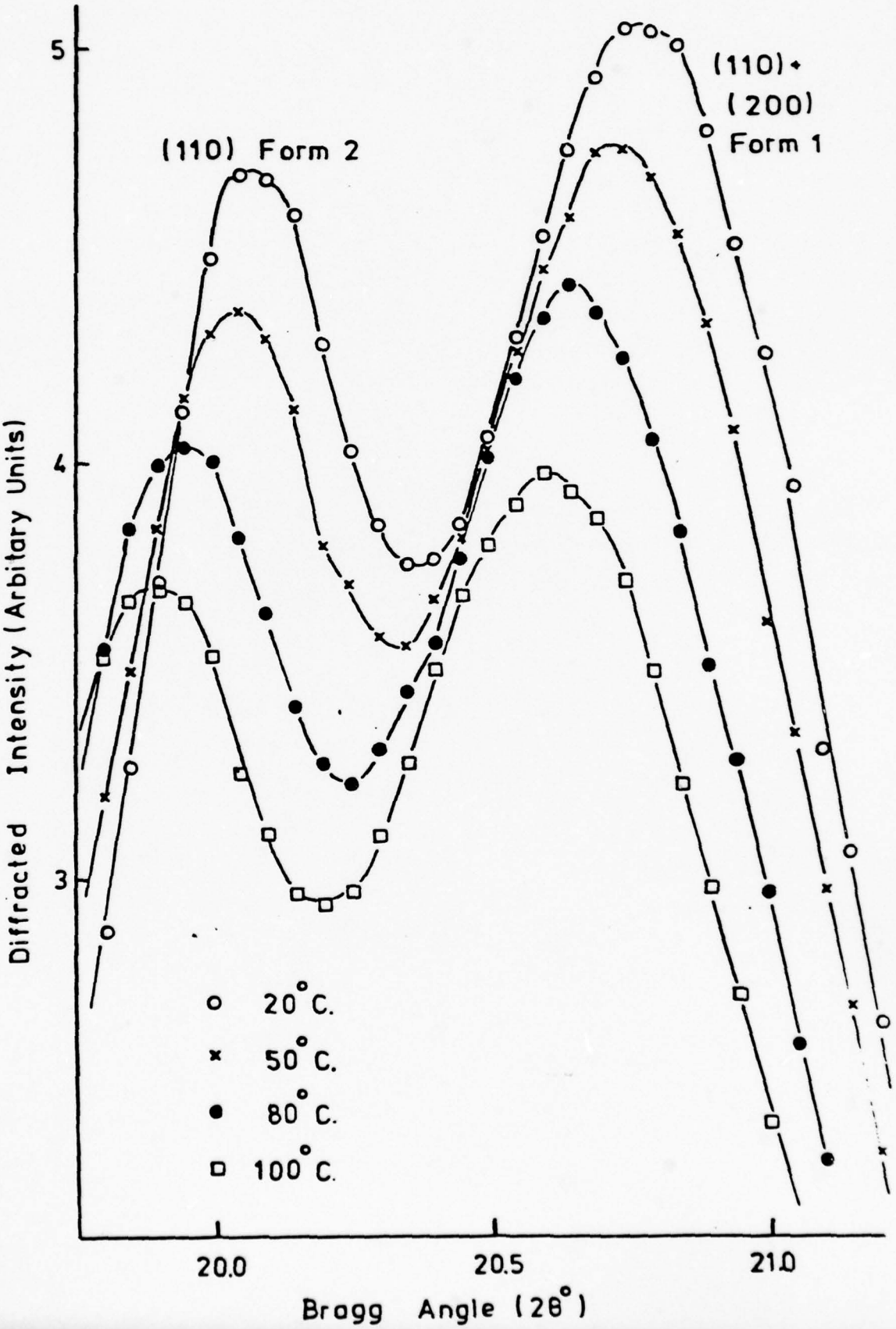

Figure 22:

Piezoelectricity against Corona Charging Time for a Surface Potential of 7.5 KV.

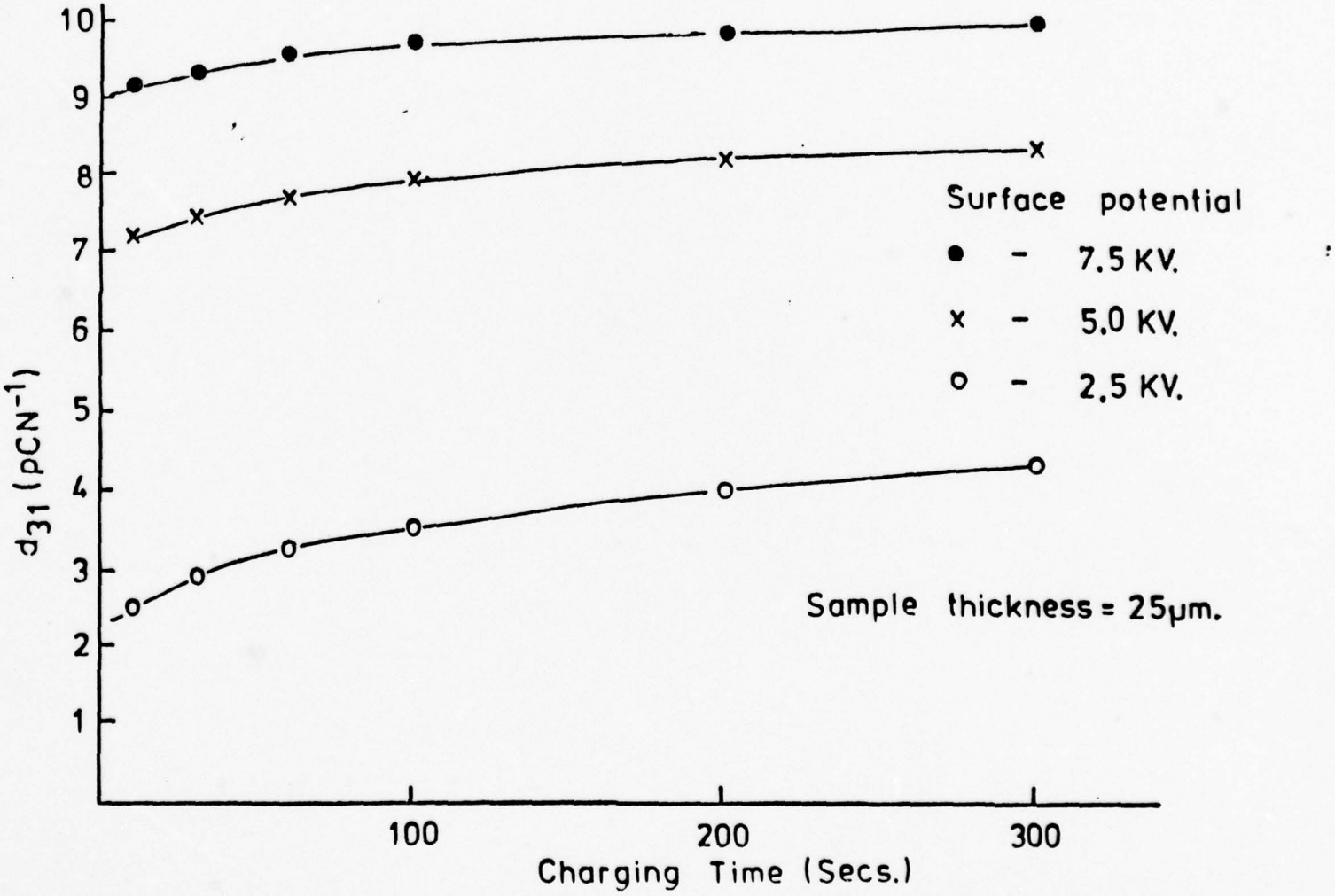

Figure 23:

Piezoelectric Activity v Poling Temperatures for various Corona Poling Fields.
Poling Time = 5mins. 25μm sample.

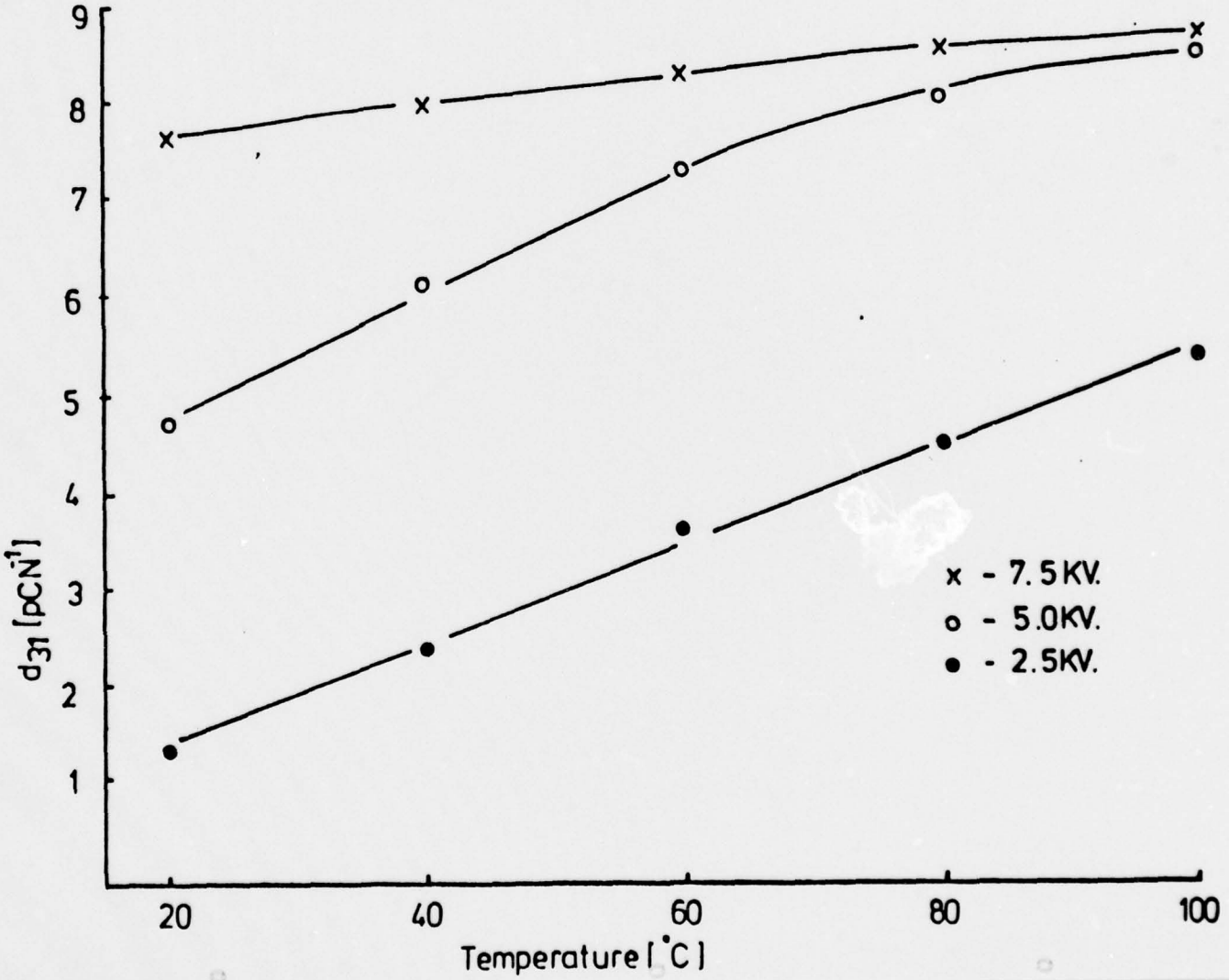

Figure 24:

Comparison of Piezoelectric Activity Due to Positive and Negative Corona

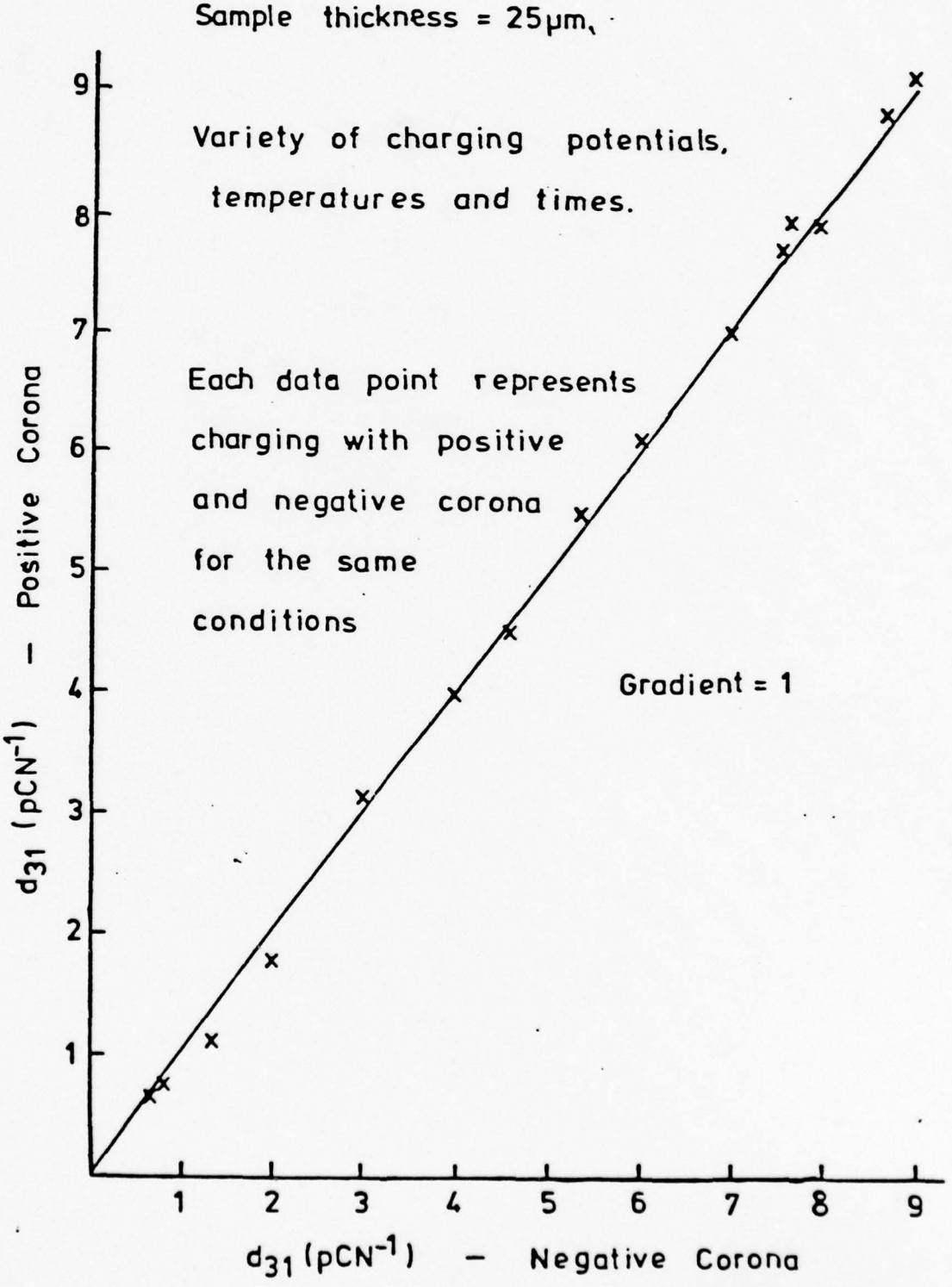

Figure 25:

Piezoelectric Response for Aluminium Electrodes v Piezoelectric Response for (a) Gold Electrodes and (b) Silver Dag Electrodes for samples corona charged to various surface potentials. 25μm samples.

o poling temperature 100° C

x poling temperature 20°C

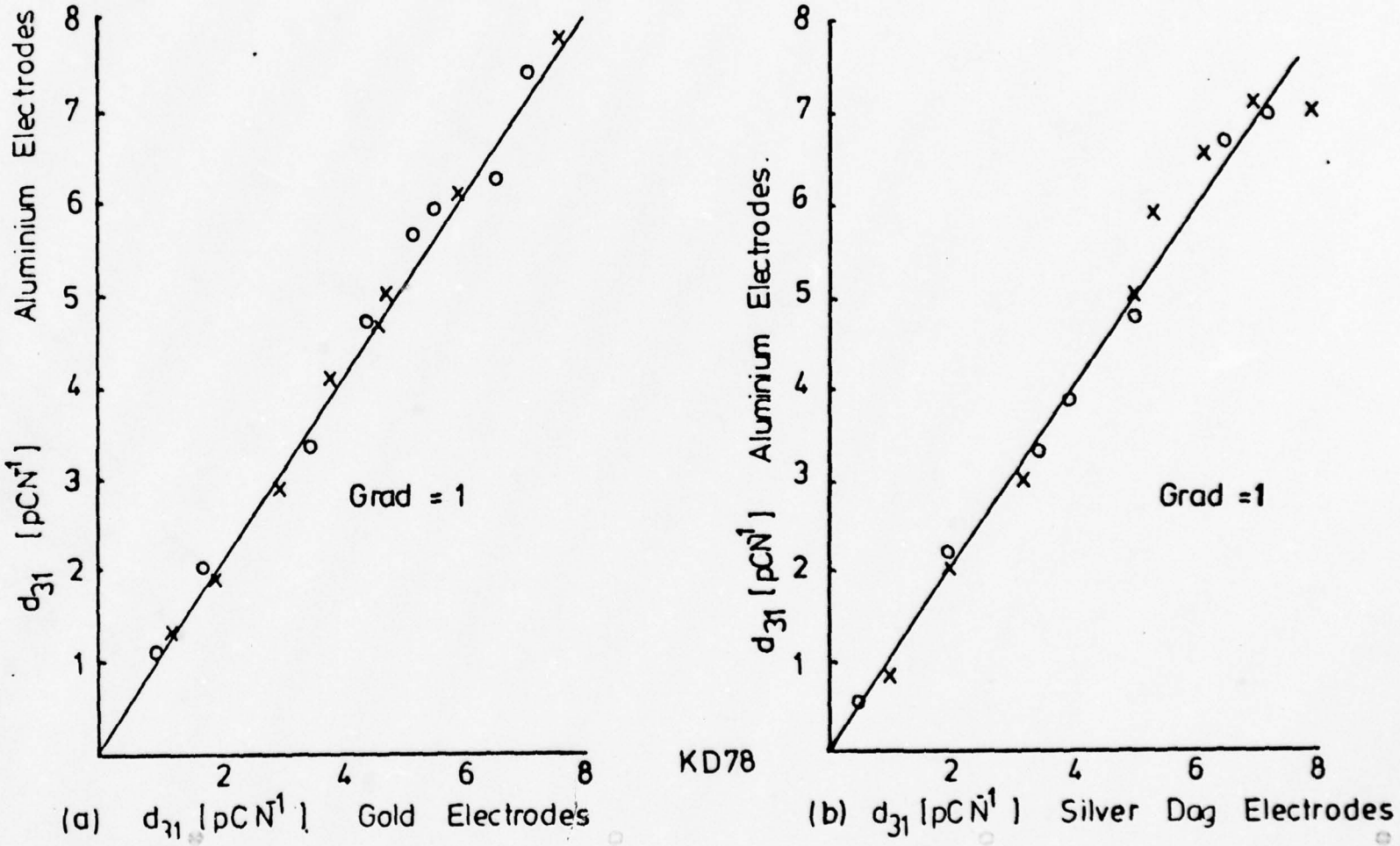

KD78

Figure 26:

To show the effect on Piezoelectricity of Cooling a charged Sample to ambient temperature before removing the corona

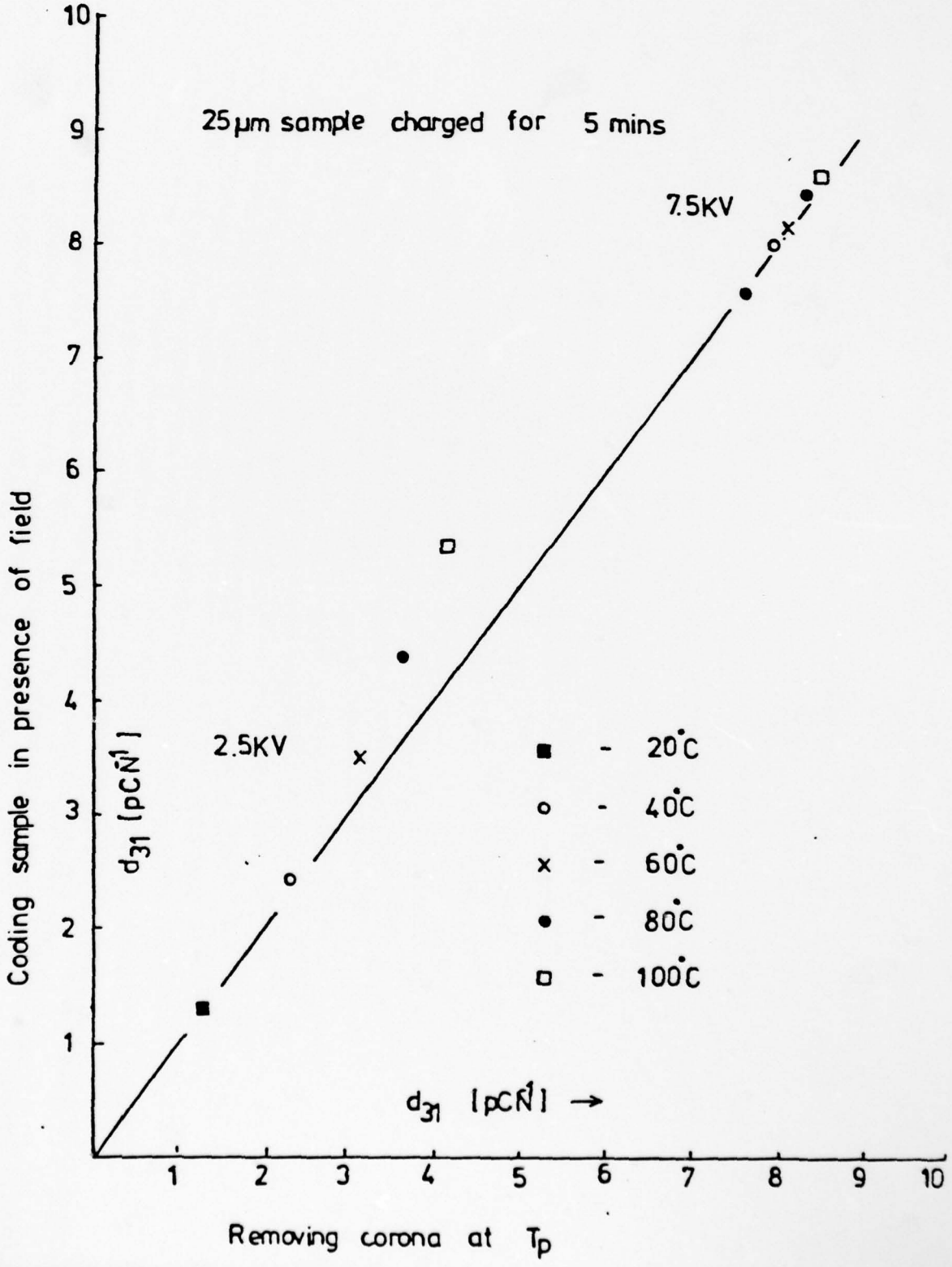

X-Ray diffraction patterns of (50 μm) PVF_2 stretched and corona charged.

Figure 27:

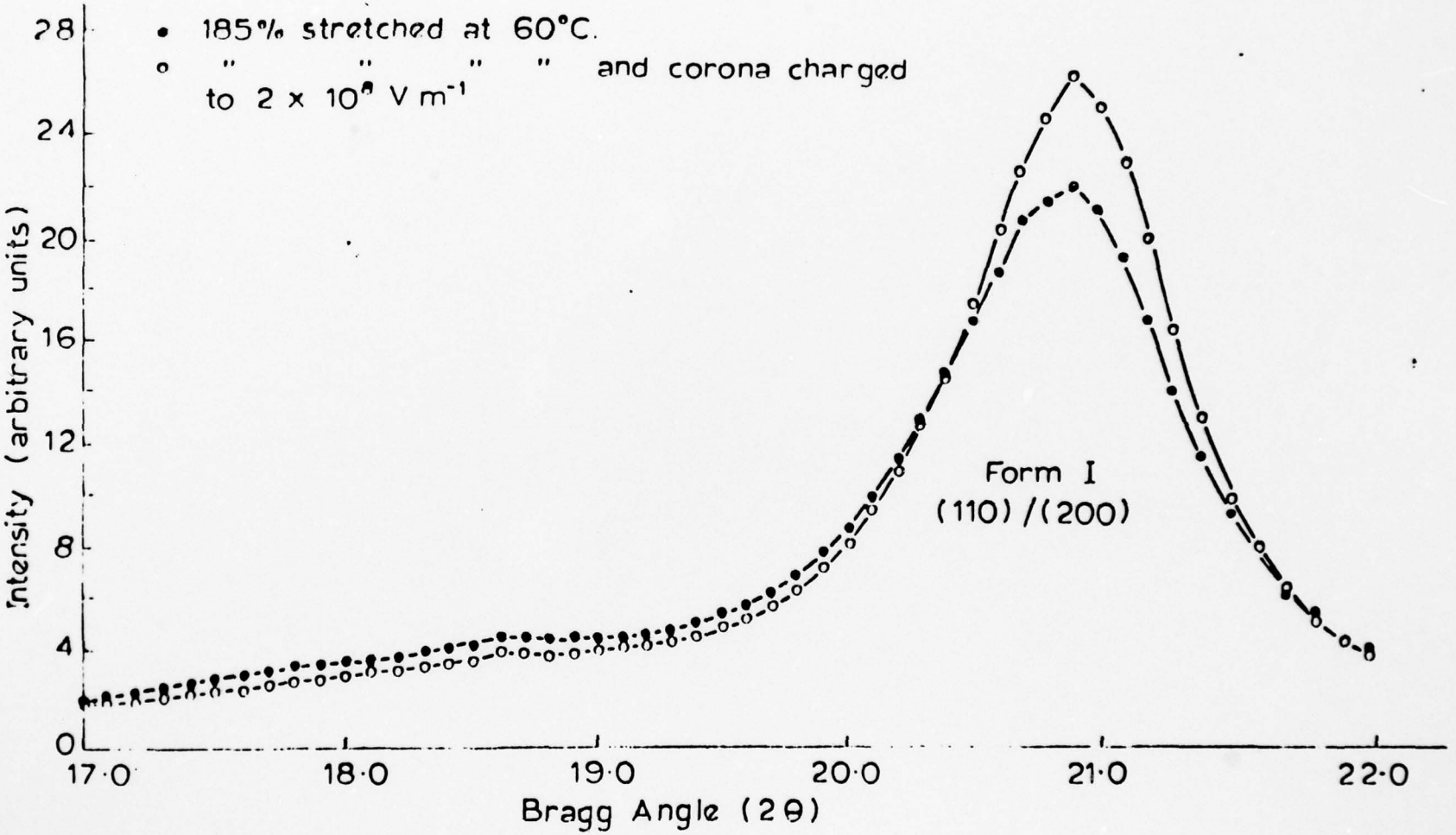

Figure 28:

Corona Charging at 100°C. of PVF_2 Stretched 5:1 at 145°C.

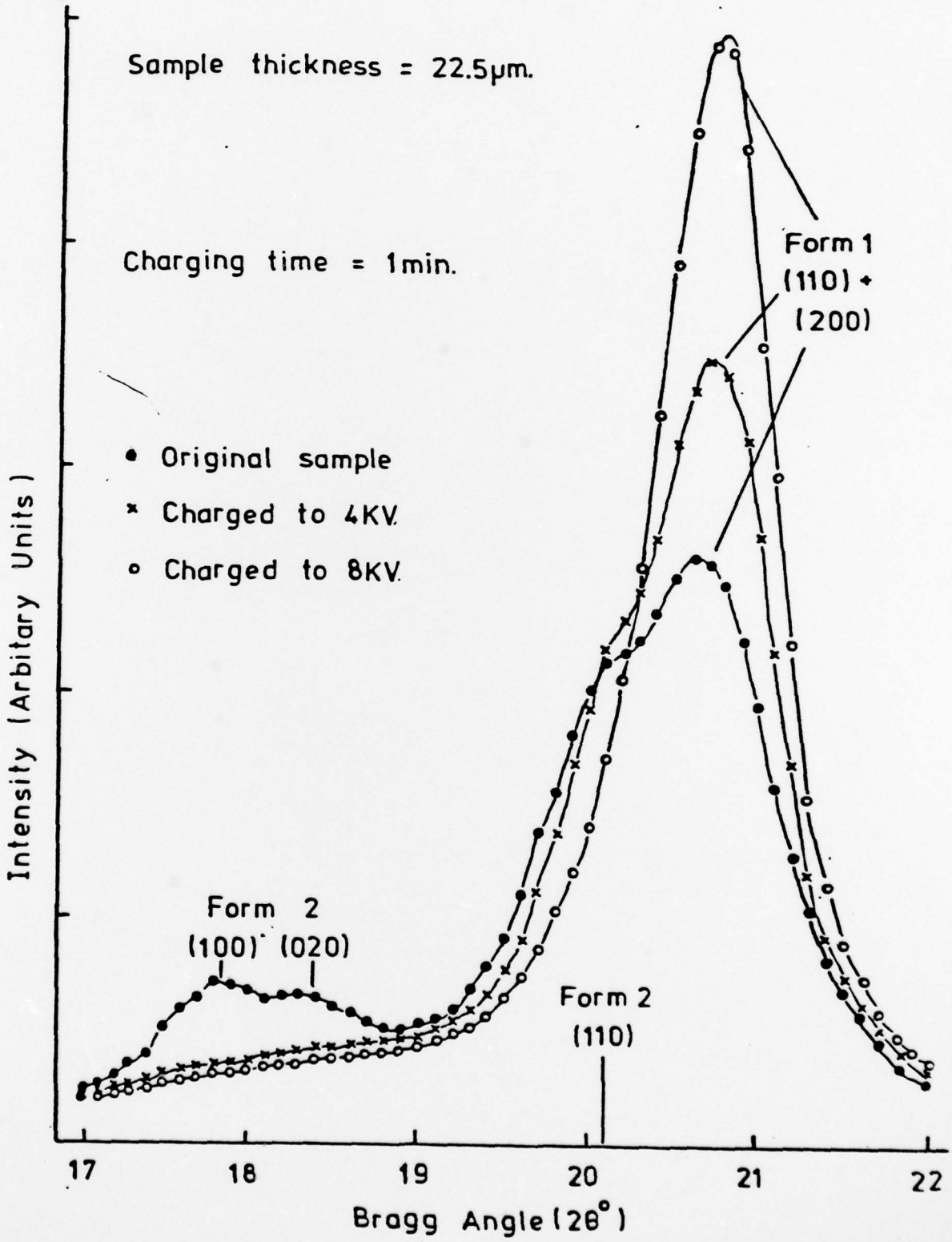

Figure 29:

Effect of Breakdown Potentials at 20°C. on Sample Stretched 5:1 at 145°C.

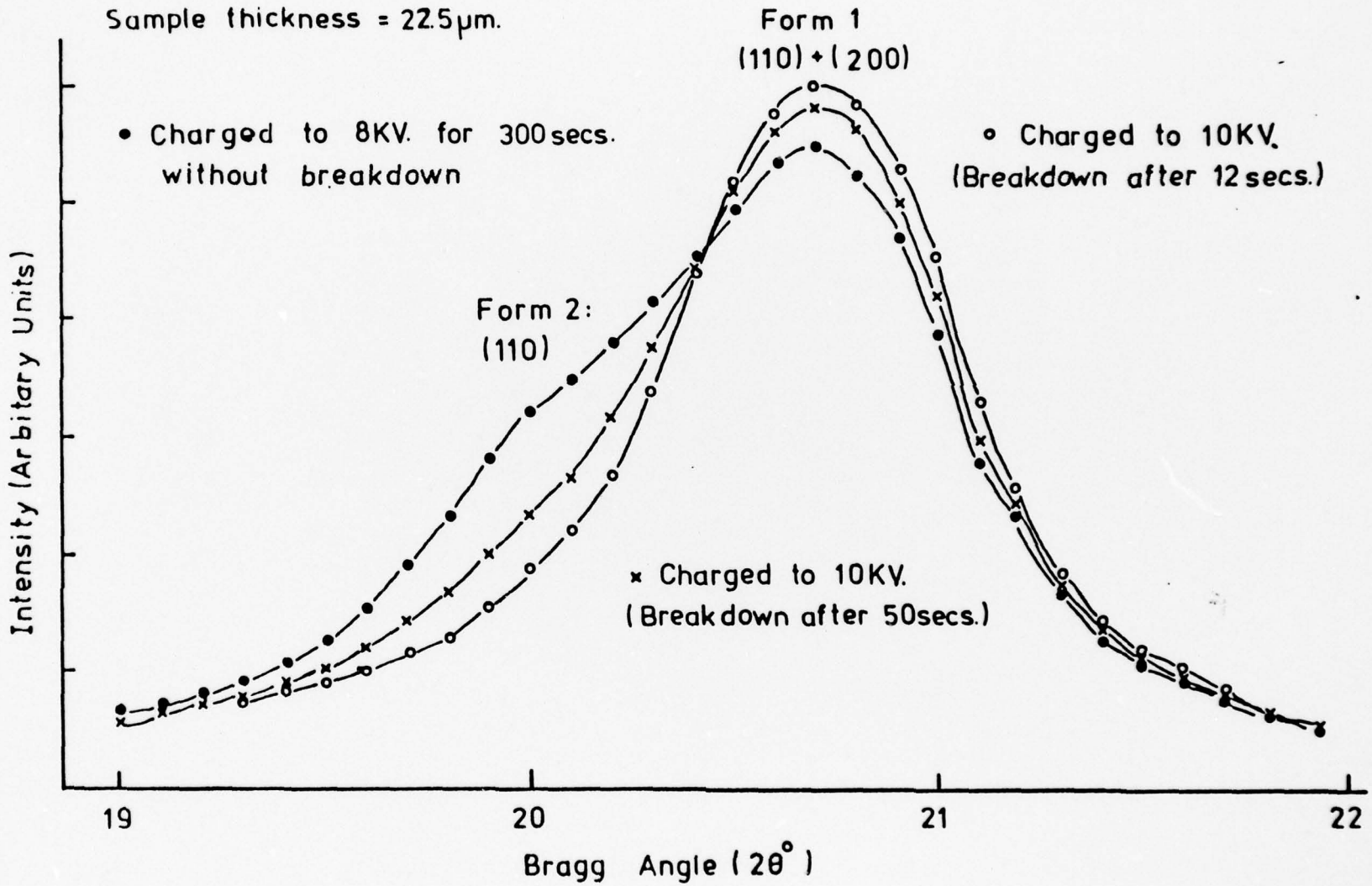

Piezoelectric strain coefficient d_{31}, of corona charged ($2 \times 10^8 V m^{-1}$) PVF_2 with different stretch ratios.
Figure 30:

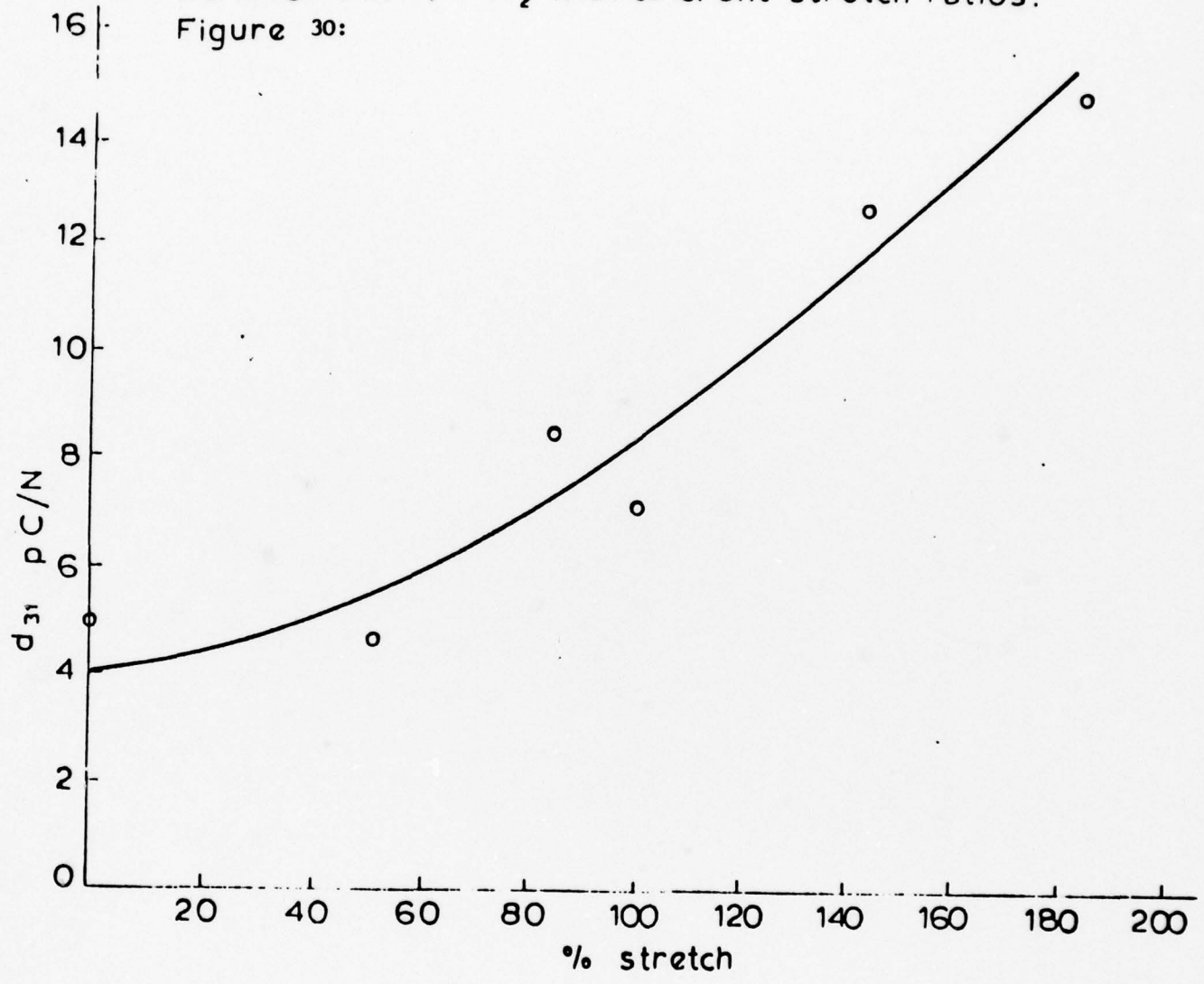

Figure 31:

Piezoelectric Activity of Stretched and Corona Charged PVF_2

Sample stretched 5:1 at 145°C. (Mixture of Forms 1 and 2)

22.5μm. thick samples corona charged for 100secs.

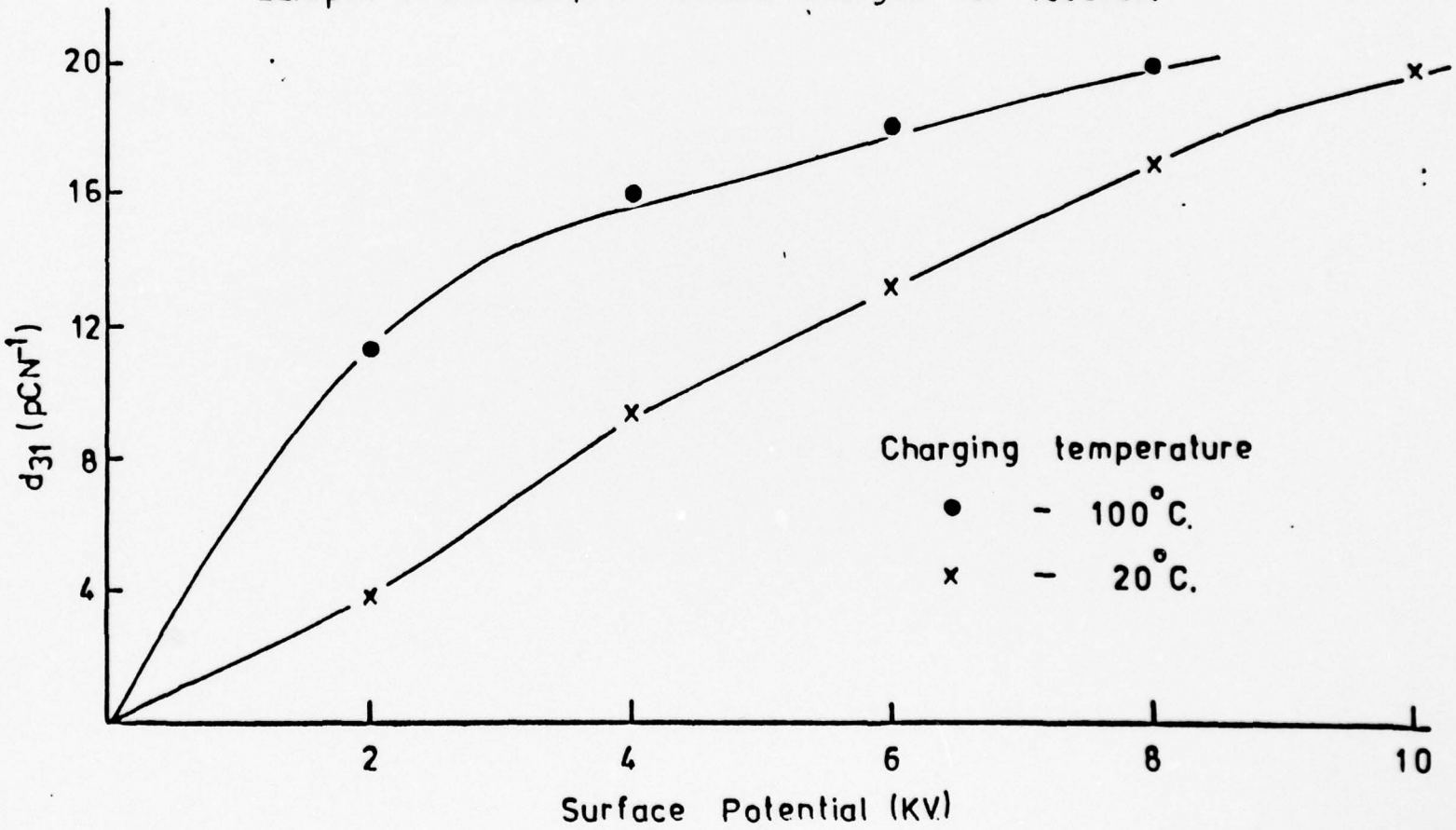

Figure 32:

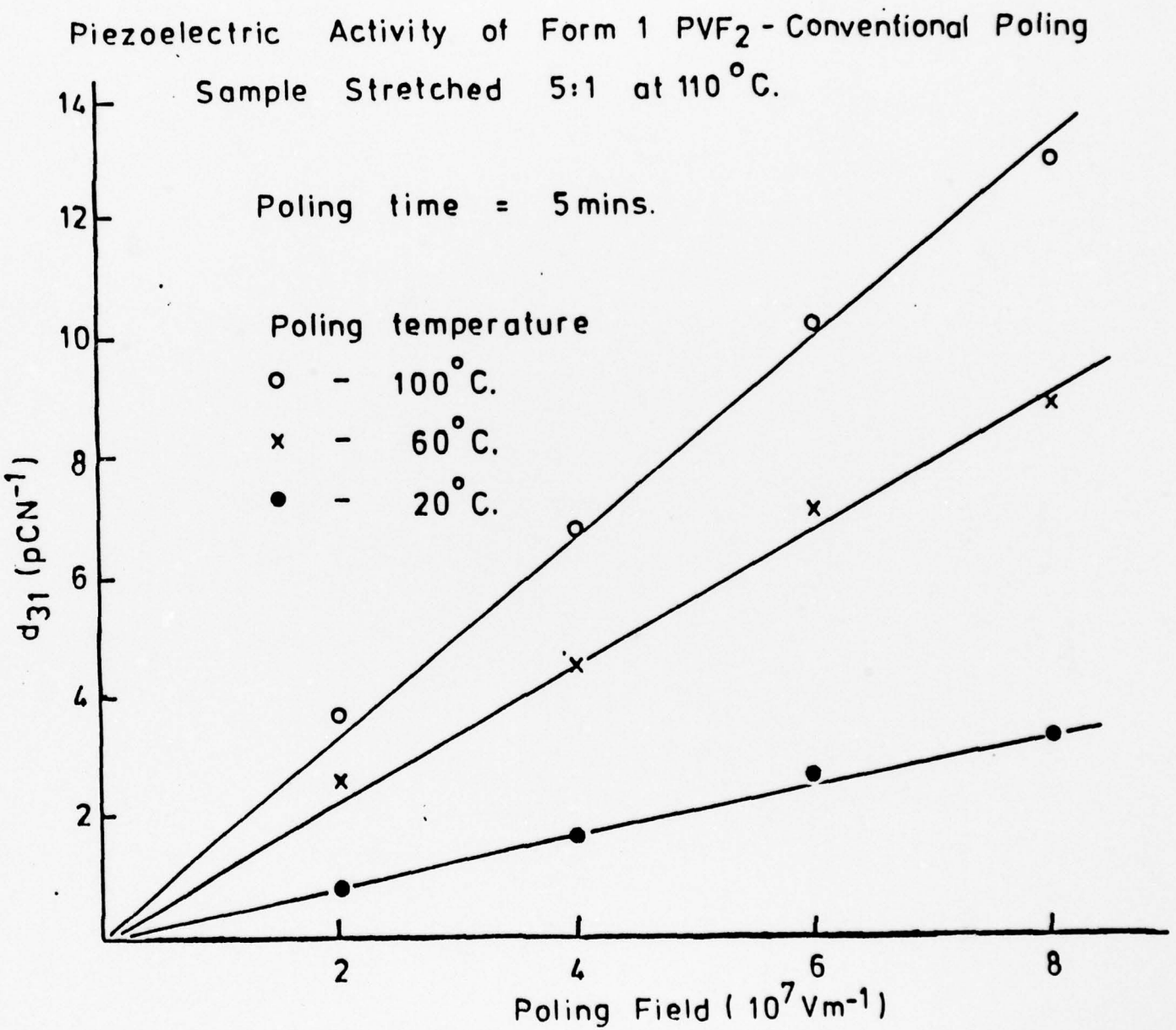
Piezoelectric Activity of Form 1 PVF_2 - Conventional Poling
Sample Stretched 5:1 at 110 °C.
Poling time = 5 mins.
Poling temperature
o - 100 °C.
x - 60 °C.
● - 20 °C.
d_{31} (pCN^{-1})
14
12
10
8
6
4
2
2
4
6
8
Poling Field ($10^7 Vm^{-1}$)

Figure 33:

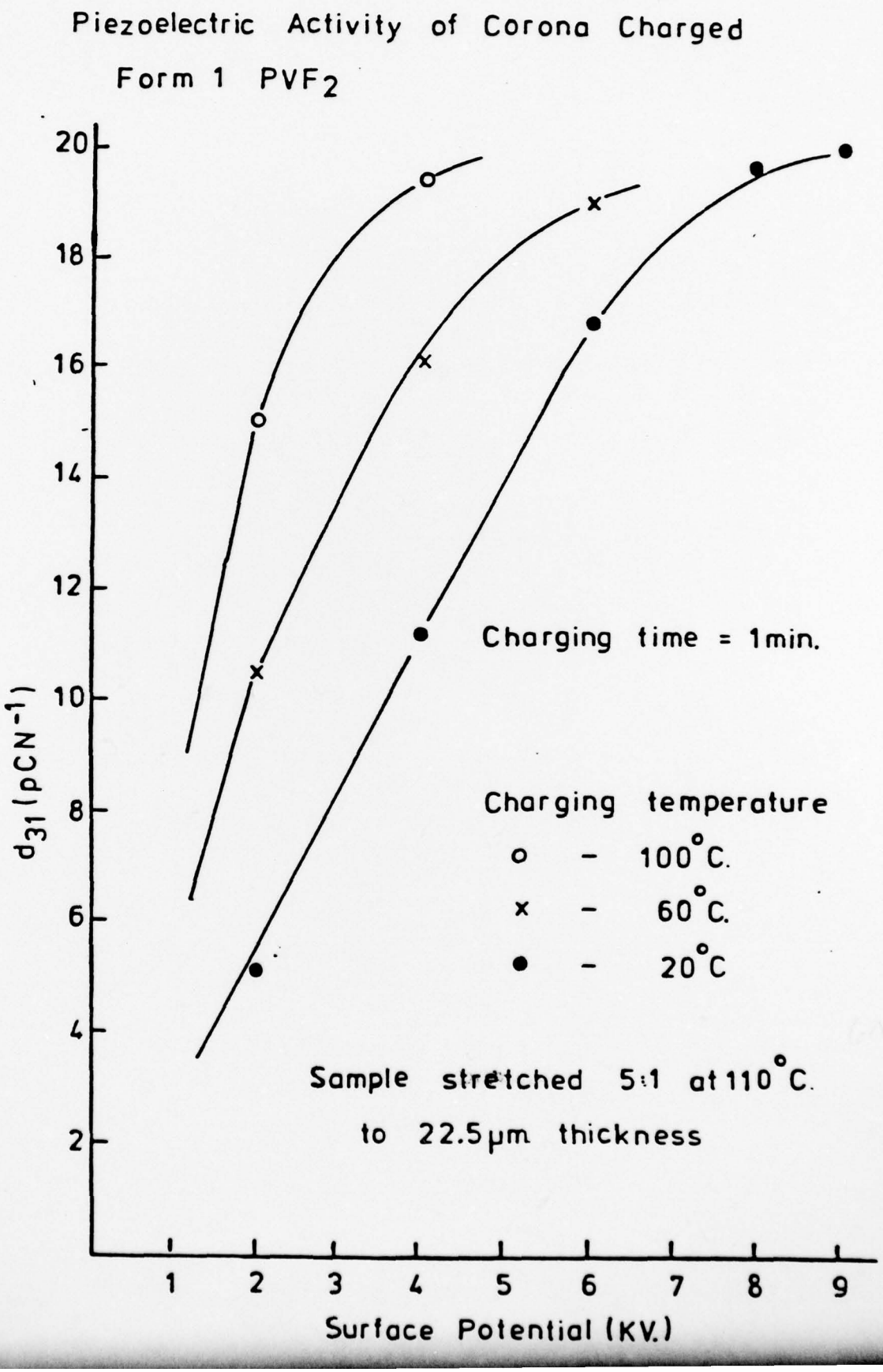
Piezoelectric Activity of Corona Charged
Form 1 PVF2
20
18
16
14
12
10
8
6
4
2
d31 (pCN-1)
Charging time = 1min.
Charging temperature
o - 100°C.
x - 60°C.
• - 20°C
Sample stretched 5:1 at 110°C.
to 22.5μm thickness
1
2
3
4
5
6
7
8
9
Surface Potential (KV.)

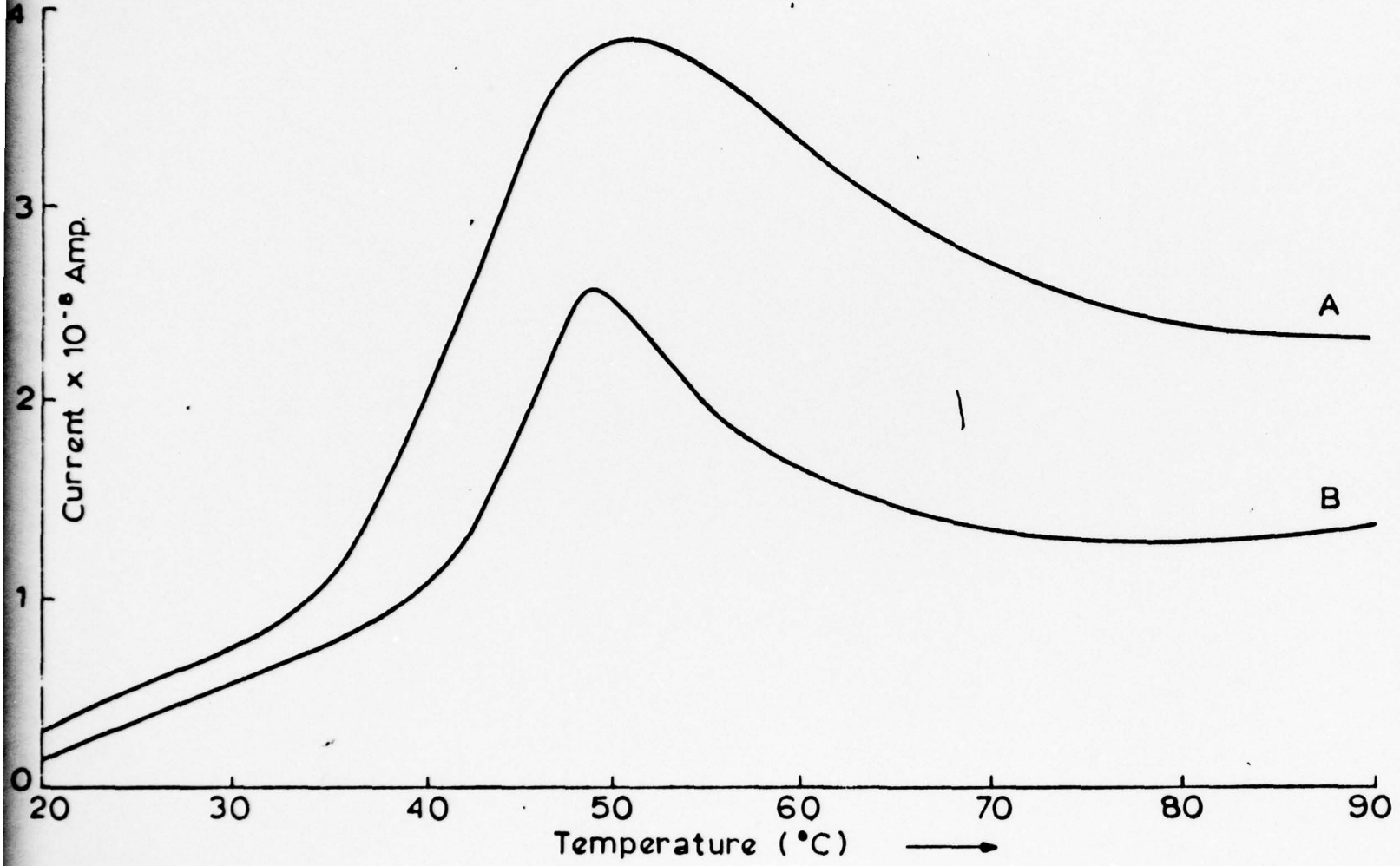

Figure 34:

Figure 35:

Pyroelectric Coefficient as a Function of Temperature for Different Corona Charging Voltages - 100sec. charging at 20°C.

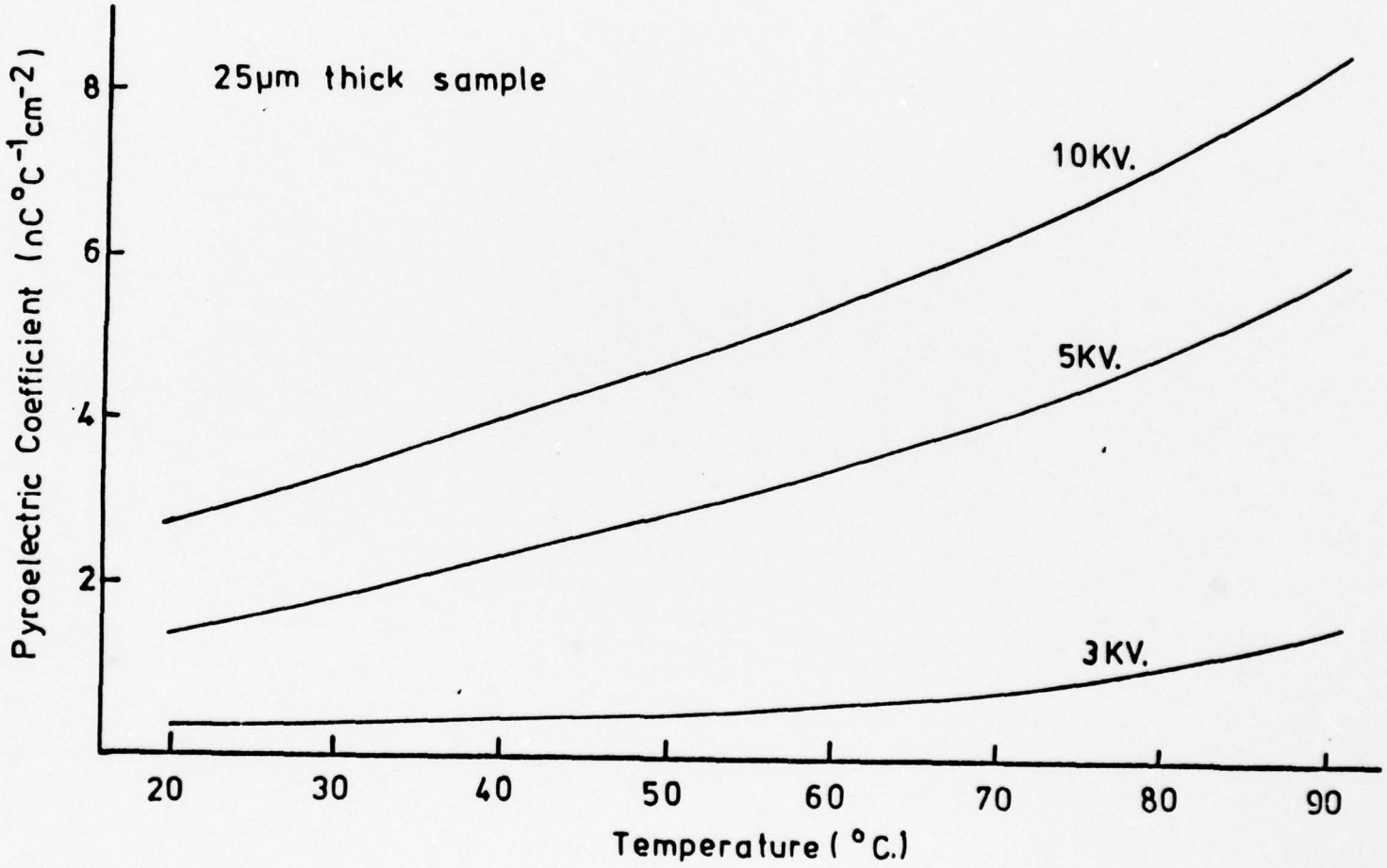

The experimental arrangement to obtain light scattering patterns in the H_v mode (crossed polarizers).

Figure 36:

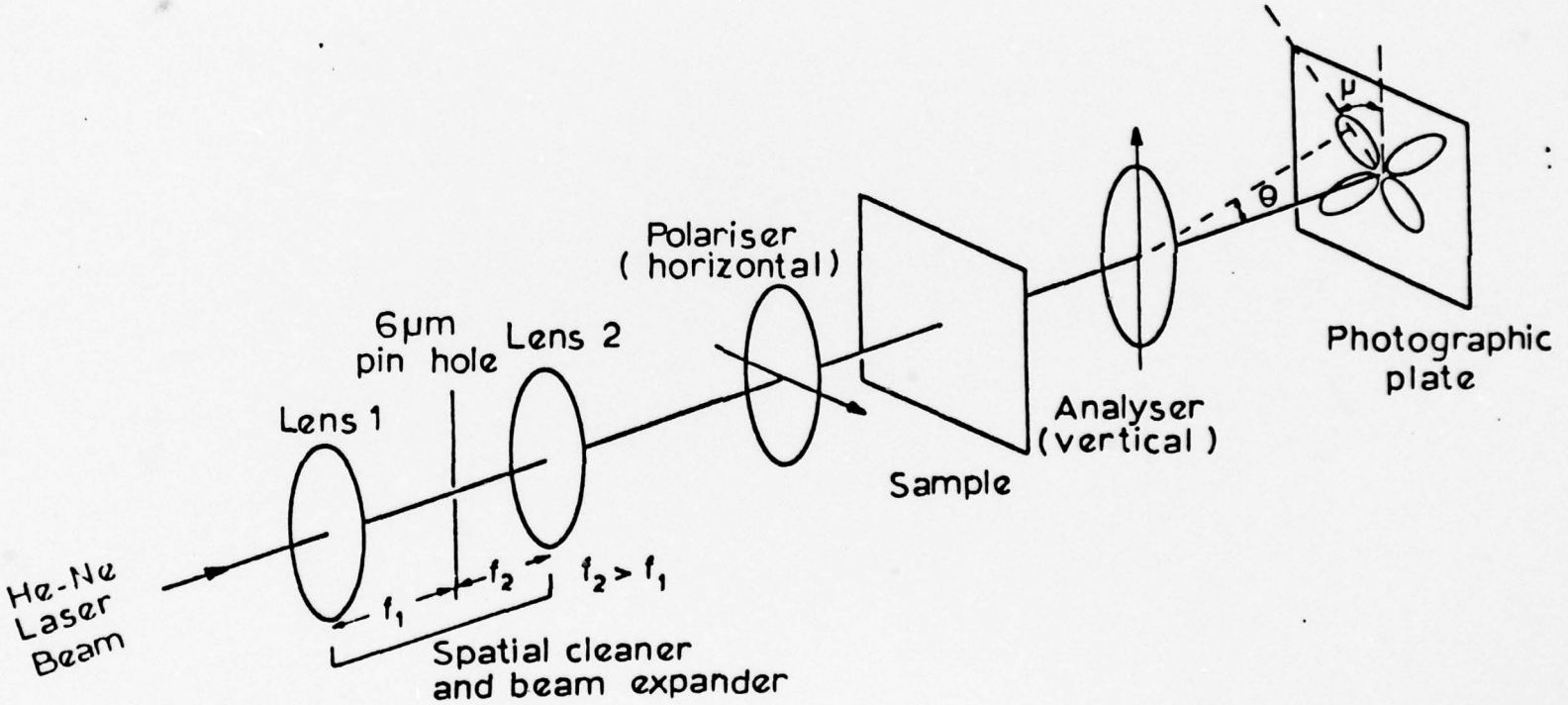

Birefringence of PVF_2 with different stretch ratios.

Figure 37:

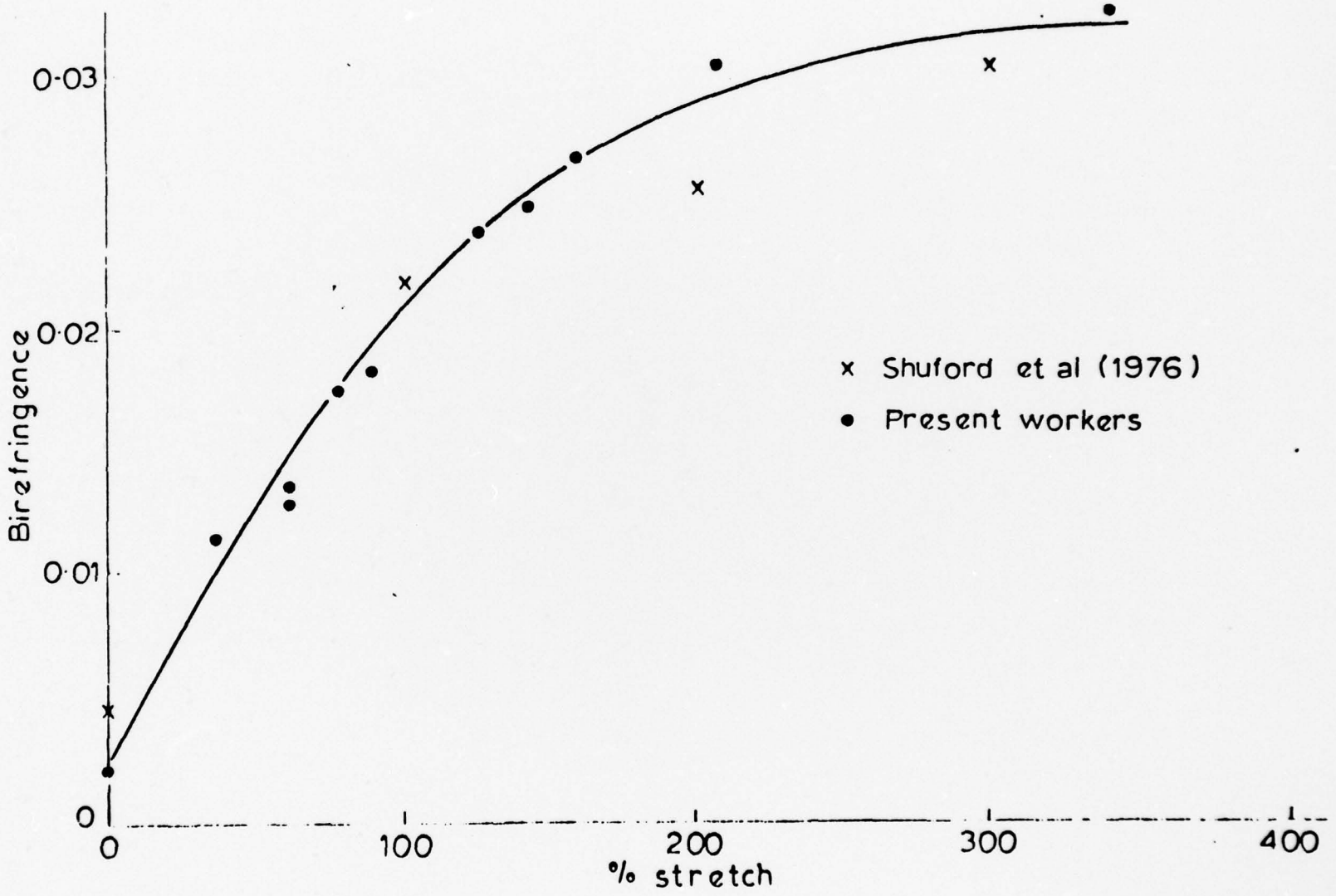

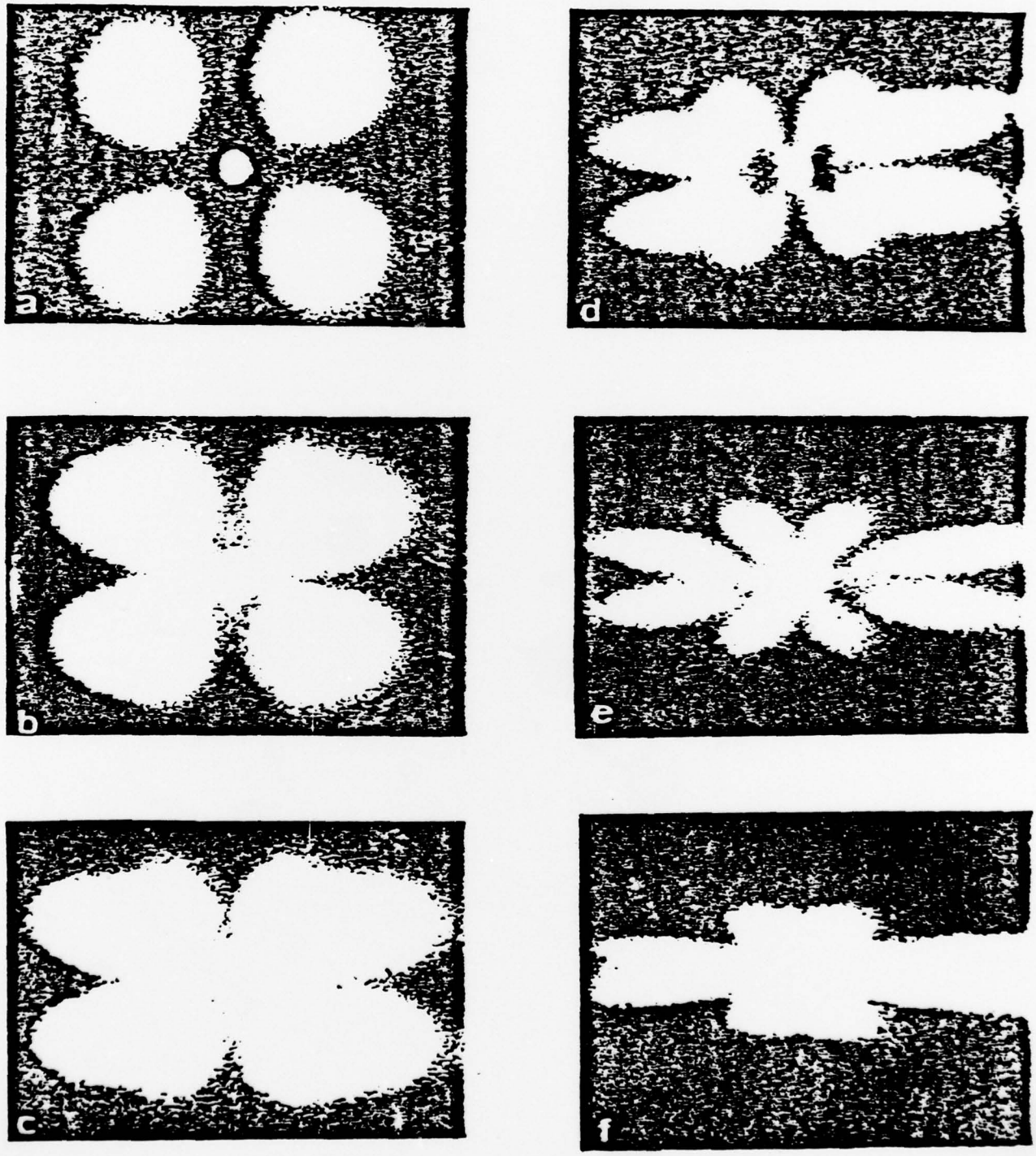

Fig. 38: Small Angle Light Scattering Patterns (SALS) of PVF_2 with different stretch ratios.
a, b, c, d, e and f represent no stretch, 10%, 30% 60%, 95%, and 140% stretch ratios respectively.

Suggested intermediate form
after corona charging.
Figure 39;

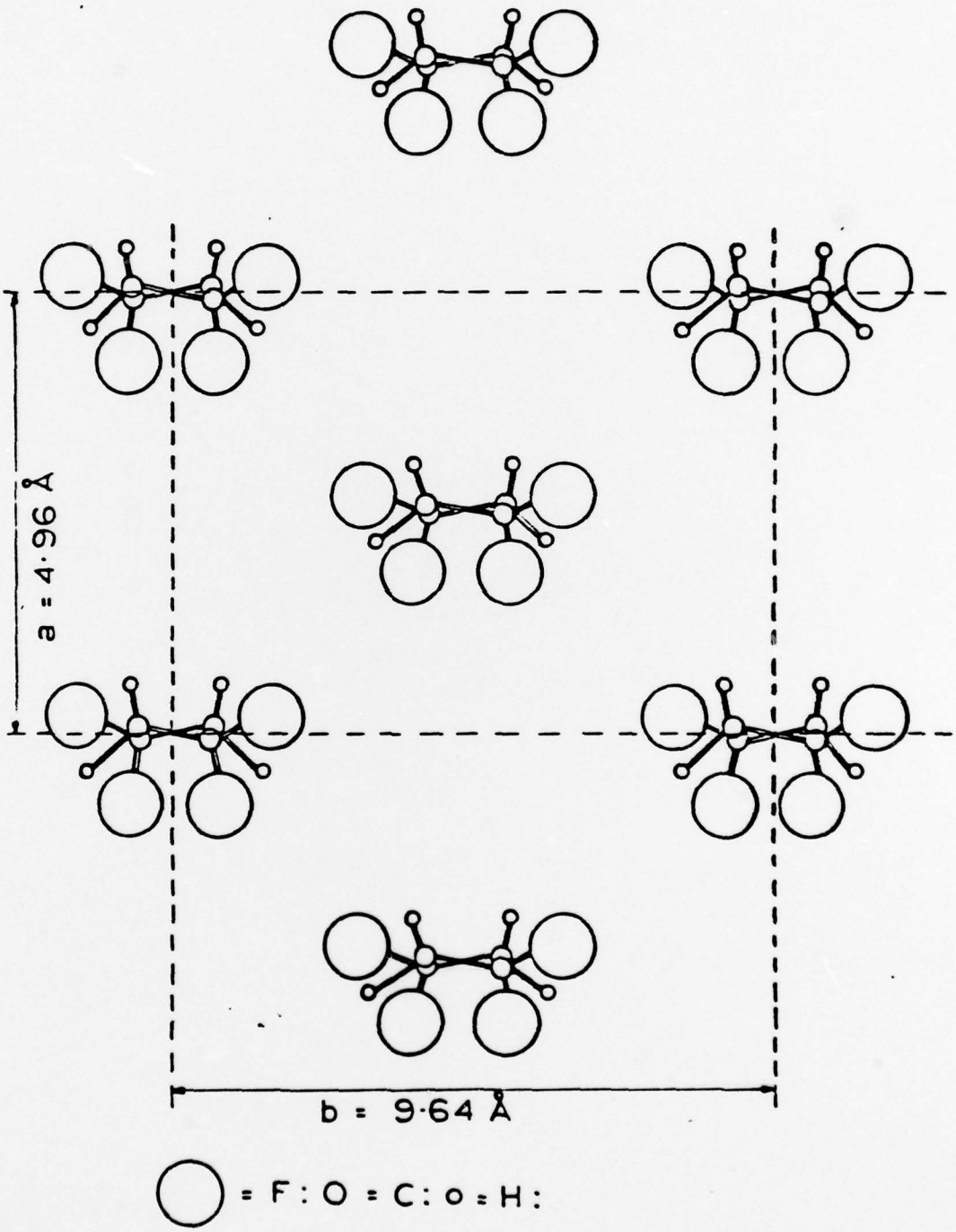

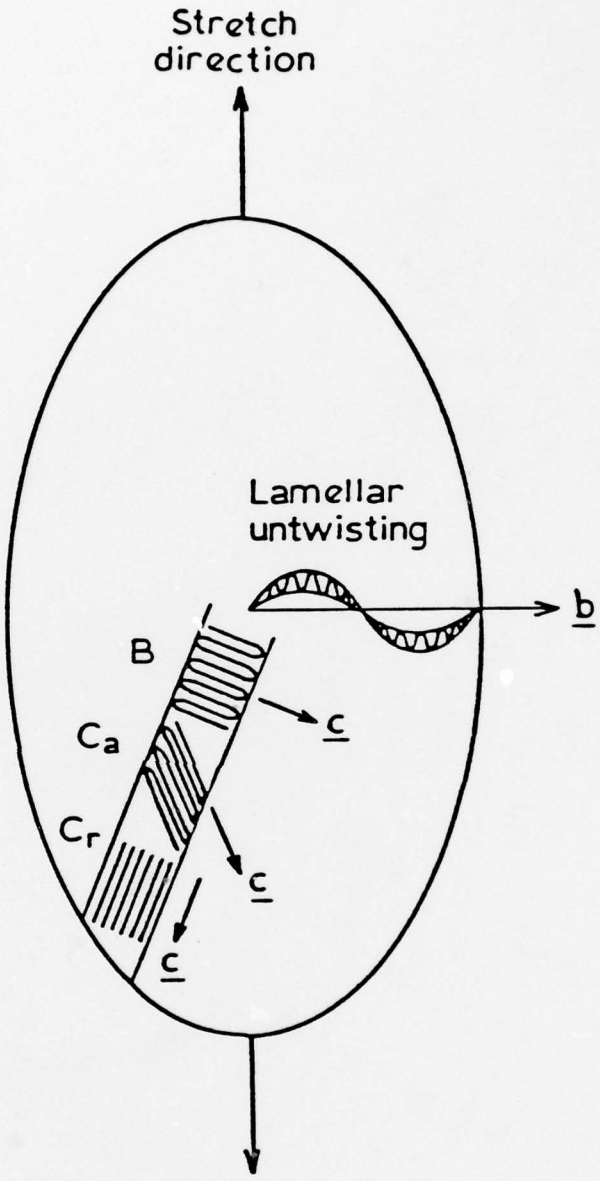

Figure 40: